BENCHMARKING AND CHARACTERIZATION OF THE RPI LSDS FOR SPENT FUEL ASSAY

By

Adam D. Weltz

A Thesis Submitted to the Graduate
Faculty of Rensselaer Polytechnic Institute
in Partial Fulfillment of the
Requirements for the degree of
MASTER OF SCIENCE
Major Subject: Nuclear Engineering

Approved by the
Examining Committee:

____
Yaron Danon, Thesis Advisor

____
George Xu, Thesis Advisor

____
Wei Ji, Thesis Advisor

Rensselaer Polytechnic Institute
Troy, New York

February, 2017
For Graduation May 2017

CONTENTS

LIST OF TABLES

LIST OF FIGURES

ACKNOWLEDGMENT

Research for this project was funded via the Material Protection, Accounting, and Control Technology (MPACT) campaign under the Department of Energy (DOE). Collaborators include: PNNL, Los Alamos National Laboratory (LANL), University of Nevada Las Vegas (UNLV), Rensselaer Polytechnic Institute (RPI), and Idaho State University (ISU).

Research at the Gaerttner LINAC Center and RPI as a whole are cooperative efforts strengthened by internal and external collaborations. I'd like to express gratitude to each and every faculty and staff member that made these studies possible, enjoyable, and especially trying. Chiefly, Dr. Yaron Danon provided direction and expertise throughout this research project. In addition, Dr. Bjorn Becker, Dr. John Kulisek, and Dr. Glenn Warren were instrumental in the collaborative effort of this research. A special thanks to the LINAC staff, technicians and fellow research assistants—who remain dependable and gifted resources.

Lastly, I'd like to thank my parents, Jim and Dana Weltz, my brother, James Weltz, and my grandparents, Dan and Nancy Austin for their support and inspiration.

ABSTRACT

The Department of Energy's MPACT Campaign funded a collaborative initiative in order to demonstrate the feasibility of Lead Slowing-Down Spectroscopy (LSDS) for the assay of individual fissile isotopes—i.e. ^{235}U, ^{239}Pu, and ^{241}Pu—in spent nuclear fuel (SNF) assemblies. Such a development would be valuable for nuclear safeguards operations, including the transportation, storage, and reprocessing of SNF. Previous experiments with the RPI LSDS involved the investigation of fresh uranium fuel samples containing ^{233}U and ^{235}U. The contribution of the research presented here is the experimental demonstration of the sensitivity of the LSDS assay method to incremental quantities of fissile U and Pu. These measurements utilize a fresh nuclear fuel pin and distinct ^{235}U and ^{239}Pu samples in order to better mimic the composition of SNF. The experimental data analysis algorithms were developed at PNNL, which were used to quantify the individual isotopic fissile masses of ^{235}U and ^{239}Pu. A linear empirical algorithm—applied to seven fissile configurations with a total ^{235}U and ^{239}Pu mass up to 37.4g and 138g, respectively—performed best and resulted in a root-mean-square error of 2.7% for ^{235}U and 6.3% for ^{239}Pu mass determination. Additional work is necessary to demonstrate a proof of principle for the isotopic assay of SNF assemblies using LSDS, but the experimental results present here demonstrate progress towards that goal.

1. INTRODUCTION

1.1 Spent Nuclear Fuel: Composition, Storage, and Assay

The risks and challenges facing the nuclear power industry can be broken down into three categories: operational safety, waste management, and nuclear nonproliferation [1]. While improved reactor designs and adapted safety policies have improved the safety of reactor operation, there is presently no resolution to the permanent storage or treatment of SNF in the United States. In fact, the aggregate of more than 75,000 metric tons of commercial light water reactor (LWR) SNF is contained on site at U.S. reactor facilities in interim storage (in pools or dry casks), and total increases by 2,000 to 2,400 metric tons annually [2].

Spent fuel from a typical LWR fuel cycle is composed of approximately 0.8-wt% ^{235}U and 0.5-wt% fissile Pu (^{239}Pu and ^{241}Pu) [3], [4]. This special nuclear material (SNM), which the United States Nuclear Regulatory Commission (U.S.NRC) defines as plutonium and uranium enriched in ^{233}U or ^{235}U, poses a proliferation concern due to its fissile nature [5]. Nuclear safeguards are currently in place to reduce the risk of proliferation; however, these methods depend on material accountability, which is limited by the accuracy of current assay methods used to characterize the SNM in spent nuclear fuel [6].

Assay refers to any number of tests, trials, or analyses which aim to determine the quality or quantity of an analyte [7]. Analytical chemistry has long been used to precisely determine the chemical composition of materials; however, the chemical breakdown of SNF is undesirable due to the volatile and robust radioactivity of activation and fission products within the material. Therefore, a direct assay method for the purpose of determining the fissile composition of SNF should be nondestructive, as destructive analyses are not a viable option for the bulk assay of large SNF stockpiles.

Considering that much of the world's Pu currently exists in SNF (in the form of 17x17 LWR spent fuel assemblies in the U.S., there is significant motivation to develop a direct, NDA method for the quantification of fissile material (^{235}U, ^{239}Pu, and ^{241}Pu) in this form. In fact, the development of direct, non-destructive, and independent method for the assay of bulk fissile material (specifically, SNF) is a goal of the Office of Nuclear Energy, Fuel Cycle Research and Development, and Material Protection and Control Technology (MPACT) Campaign [8]. Such a development would be a benefit to nuclear safeguards, nuclear material accountability, and SNF reprocessing, storage, and transportation efforts [9], [10].

A cooperative research group from University of California Berkley outlined eight advantages associated with the improvement of current methods for SNF assay [11]. (1) Providing regulators with the capability to independently verify Pu mass onsite. (2) Providing public confidence regarding SNF shipment. (3) Providing continuity of knowledge at any SNF site. (4) Allowing reactor operators to optimally reload reactor cores. (5) Providing the capability to optimally pack fuel for transport, interim, and long-term storage. (6) Enabling the determination of input quantities of nuclear material for reprocessing methods. (7) Promoting cost savings by facilitating assembly selection for reprocessing. And (8) enabling the determination of shipper/receiver differences of Pu mass.

The shipper/receiver difference refers to the potential of an unwanted diversion of special nuclear material during the transportation of SNF. In the last 40 years, thousands of shipments of SNF have been transported in The United States [12]. These shipments are closely overseen by the U.S.NRC and Department of Transportation, and the safe shipment of nuclear material is achieved by a combination of factors, including physical properties of the material, ruggedness of the container, and overall operating procedures [13]. While there has never been a radiological release during the transportation of SNF in the U.S., there is a current inability to demonstrate that nuclear material has not been diverted during transit. The solution to this shortcoming requires the assay of SNF before and after shipment with a direct method which is sensitive to internal fuel pins. This development is a primary motivating factor in the research of NDA assay techniques and would improve nuclear safeguards and reduce the risk of proliferation by demonstrating material accountability.

1.2 Techniques and Challenges of SNF Assay

The employment of chemically destructive assay techniques for SNF require specialized laboratories and involve the dissolution of the used fuel within a hot cell using heated nitric and hydrofluoric acids. Out of the large quantity of liquefied fuel, only a small aliquot of the dissolved solution is taken for analysis. This sample is diluted to reduce the radioactivity of the sample in order to be transported to a mass spectrometer, a process which introduces uncertainty into the measurement. Additional uncertainty of these radiochemical processes stems from potential incidental losses of materials during radiochemical manipulations, e.g. sample weighing, etc. Therefore, while the uncertainties associated with this method are small, they can be difficult to quantify [14]. However, the aforementioned destructive assay of SNF is not viable for the large quantities of SNF stored and transported in the U.S. Therefore, an ideal method for the assay of SNF would be nondestructive and independent, i.e. not require calibration to a previously characterized assembly.

The direct, nondestructive assay of SNF is a serious challenge due to the immense gamma-ray dose from fission products and the large neutron background from spontaneous fission and (α,n) reactions associated with the material [15]. Therefore, currently implemented NDA methods for SNF assemblies utilize computer simulation of nuclear fuel burnup which are benchmarked using destructive radio-analytic assay [14]. Passive gamma spectroscopy is used to supplement these simulations by identifying individual radioisotopes within the SNF, e.g. ^{137}Cs and ^{244}Cm [16]. The International Atomic Energy Agency (IAEA) has determined that this method has an associated Pu uncertainty of roughly 10% [17], [18].

In addition to the large Pu uncertainty, the aforementioned assay method—which integrates burnup simulations with the passive gamma detection—provides other downfalls. Principally, the comprehensive burnup history of spent fuel is not always available. Furthermore, it is often difficult to keep track of burnup information when assemblies are moved within or amongst reactor facility(s), a problem complicated by the diminishing space in spent fuel pools [9]. Additionally, the implementation of passive gamma spectroscopy is complicated by the diverse profile of background radiation emitted by SNF. Lastly, the photon attenuation (self-shielding) of the assembly makes this method insensitive to the internal pins in spent fuel assemblies. Therefore, passive gamma spectroscopy doesn't provide assay information about internal fuel pins and cannot be employed to investigate the diversion of individual SNF pins.

1.2.1 Previously Investigated Methods of SNF Assay

There are numerous methods being researched for the non-destructive assay of fissile material; some have demonstrated the capability to do so accurately [11]. Many of these techniques have been explored for their potential adaptation for SNF assembly assay. However, the physical principles and operating procedures of such methodologies that drive these independent systems lead to characteristic limitations. Eight previously demonstrated NDA techniques were investigated and are briefly described and compared for their potential adaptation for independent assay of used LWR assemblies:

1.2.1.1 Delayed Neutron Shufflers

Shufflers were conceived in 1969 at Los Alamos National Laboratory and were originally built to non-destructively assay U samples. These devices have demonstrated the ability to assay samples containing at least 10 grams of ^{235}U such as: uranium ore, scrap, waste, irradiated fuel, and MOX fuel. Shufflers operate by introducing a neutron source—typically ^{252}Cf—in order to irradiate the fissile sample and induce fission. The subsequent removal (shielding) of the source, allows for delayed neutrons to be counted in the presence of a relatively small neutron background. The shuffling of the system refers to the repetitious introduction and removal of the neutron source. Shuffler adaptation for SNF assay is complicated by internal neutron production in the form of (α,n) reactions and ^{244}Cm spontaneous fission. The former has a multiplicity of one; however the latter emits multiple neutrons and can prevent a shuffler from accurately determining the fissile mass from fission neutron multiplicity [19].

1.2.1.2 Differential Die Away

The differential die away (DDAA) method employs a combination of passive and active neutron measurements to detect the presence of fissile materials. Passive coincidence counting allows for the determination of the spontaneous fission rate from ^{240}Pu, ^{244}Cm, and ^{252}Cf isotopes and the subsequent fast neutron multiplication. Active neutron interrogation involves the repetitious irradiation of fuel sample with neutron pulses to induce fission with thermal neutrons, providing information such as the prompt neutron yield, delayed neutron yield, and coincidence prompt neutron yield in order to determine the fissile content of the sample. This has been extensively researched for the application of cargo containers, as it is a very sensitive technique for detecting ^{235}U and ^{239}Pu [20].

There are significant challenges involved with the adaptation of DDAA for used fuel assemblies. For instance, the unwanted thermal absorption of interrogation neutrons, as well as moderation effects of the fast neutrons within the SNF assemblies and reflection of neutrons from surfaces would challenge the precision of the measurements. More significantly, the unwanted pileup of neutron events during coincidence detection due to spontaneous fission sources in SNF leads to uncertainty in the ability to distinguish induced fission events. The adaptation of this system for used fuel assay also requires a standard measurement sample in order to calibrate the system to a known SNF assembly [21]- [22].

1.2.1.3 Neutron Multiplicity Counting

Passive neutron multiplicity counting is a NDA technique developed as an extension of neutron coincidence counting for Pu assay. This technique is used to directly determine three sample properties: effective fissile mass, self-multiplication, and the (α,n) reaction rate. Neutron multiplicity counting has been demonstrated to provide accurate measurements of Pu metal, oxide, scrap, and residues [23]. Multiplicity counting does not require calibration with standard samples and only necessitates short measurement times (15-30 minutes). However, the adaptation of this method for SNF assembly assay is complicated by neutron self-shielding. Additionally the mathematical algorithms calculate the mass of a single fissile isotope in the samples are Pu, and burnup codes are required to determine the ratio of ^{235}U, ^{239}Pu, and ^{241}Pu in the used fuel sample. Therefore, this method cannot assay SNF independently. [24].

1.2.1.4 Passive Neutron Albedo Reactivity (PNAR)

PNAR utilizes neutrons produced by spontaneous fission in ^{244}Cm to induce fission in the fissile material of SNF. This technique requires two measurements with fission chambers, with and without a layer of cadmium (Cd) absorber between the fuel assembly and detectors. This Cd barrier is used to absorb low energy neutrons (<0.5 eV). The neutron count ratio of the two measurements scales with additional fissile material, indicating neutron multiplication due to fissile material. Currently, the PNAR method cannot independently assay SNF assemblies, as the initial enrichment and burnup of the fuel are prerequisite [25]- [26]. Further research is needed to demonstrate PNAR as a NDA method of fissile Pu SNF.

1.2.1.5 Self-Interrogation Neutron Resonance Densitometry (SINRD)

SINRD relies on the unique resonance cross-section structures of the fissile isotopes in SNF, i.e. ^{233}U, ^{235}U, ^{239}Pu, and ^{241}Pu. This technique utilizes spontaneous fission neutrons from ^{244}Cm to self-interrogate the spent fuel pins. The concentration of fissile isotopes in the spent fuel is determined by measuring the resonance absorption lines from corresponding isotopic fission chambers; in other words, individual fission chambers which are composed of the fissile isotope which is being investigated are used to measure fission neutrons. The concentration of ^{235}U and ^{239}Pu in the spent fuel is determined by measuring the resonance absorption lines in the respective fission chambers [27]. Additionally, fission chambers with various absorbing filters (e.g. boron carbide, gadolinium, or cadmium) to help determine the quantity of the specific fissile isotope of interest is contained in the fuel assembly.

This method has been verified for fresh and MOX fuel assay; however, adaptation of SINRD for SNF assay is limited by self-shielding. Additionally, this method would require calibration with a reference assembly. This technique is insensitive to the high gamma radiation levels in SNF and shows promise for the detection of diversion of SNF pins [28]- [29].

1.2.1.6 X-Ray Fluorescence (XRF)

The XRF assay technique focuses on the feasibility of utilizing excited x-ray emission peaks from Pu and U to infer their relative abundances in SNF. Since fluorescence is chemically-specific, XRF cannot be used to determine isotopic the ratios of Pu. Therefore, an additional burnup measurement would be required to infer the fissile Pu content. Additionally, this method has demonstrated the ability to determine the Pu content in a single fuel pin, but is hindered by the limited penetration of characteristic X-rays. The mean free path of such photons is only a fraction of a mm, so only the outer pins of a fuel assembly contribute to the detected signal. Therefore, the XRF method is blind to the diversion of pins which are not in a line-of-sight with the detector [30].

1.2.1.7 Delayed Gamma

The delayed gamma technique involves the detection of delayed gamma rays from fission-product nuclei to measure the relative concentrations of fissile material. The distribution of these fission products within a SNF assembly can be measured by gamma spectroscopy. The intensities of individual gamma peaks—once corrected for attenuation and detector efficiencies—are indicative of the fission reaction rates of a particular isotope. This method has been used to demonstrate the ability to independently and nondestructively quantify the ^{239}Pu content in SNF. Recent simulations demonstrated the ability of a high-purity germanium spectrometer, a 4×10^{10} n/s deuterium-tritium neutron source, and a 100-minute assay time to determine the quantity of ^{235}U, ^{239}Pu, and ^{241}Pu in individual PWR fuel pins with an accuracy of 7% [31]. However, the simulations made simplifications, including ignoring the contribution of fast fissions. Additionally, the buildup of Compton scattered photons was ignored, which can degrade the signal-to-noise ratio. Additionally, another inherent challenge accompanying the delayed gamma technique for spent fuel assembly assay is photon attenuation (self-shielding) within an assembly [16], [30], and [32].

1.2.1.8 Nuclear Resonance Fluorescence (NRF)

NRF measurements involve the excitation of nuclei using an external photon beam, causing the emission of gamma rays, which are characteristic to the excited isotope. This method provides the potential to identify not only the concentration of fissile isotopes, but minor actinides as well. Unfortunately, this method is limited by current source technologies. Currently, the precise determination of Pu content necessitates both large detector arrays and unrealistically long counting times due to low fluorescence signal rates and the considerable background of SNF [33], [34]. As with the other gamma methods, self-shielding severely limits the application for the assay of an assembly.

2. SLOWING-DOWN SPECTROSCOPY

Lead slowing-down spectrometry was developed in order to measure neutron cross-sections as an alternative to the time-of-flight (TOF) method [35]. While TOF provides superior energy resolution and lower background radiation, the flux within a slowing-down spectrometer is about 10^4 times larger than a conventional TOF experiment at a flight path distance of 5 meters. This allows for the measurement of small samples; LSDS has shown the capability to measure cross-sections down to ~100 microbarns when sample sizes are limited to 10's of nanograms [36], [37]. The use of an LSDS to determine various actinide cross-sections has been well documented [38]- [39].

The performance, i.e. energy resolution, of a slowing-down spectrometer is dependent on the atomic mass, absorbing characteristics, and homogeneity of the slowing-down medium. Lead (Pb) is the optimal medium because of its large atomic mass, low absorption cross-section, and availability.

The LSDS method is driven by the introduction of a pulse of interrogation neutrons within the slowing-down medium. Immediately after the initial neutron pulse is generated within the LSDS, inelastic scattering rapidly moderates the highest energy interrogation neutrons. However, elastic scattering quickly becomes the dominating reaction, as inelastic scattering on Pb has an insignificant cross section below a couple MeV. These continuous neutron scattering reactions with Pb nuclei allow for the correlation between neutron energy and time after the pulse. This correlation occurs because the most energetic neutrons will diffuse through the slowing-down medium with the greatest velocity, undergoing the most rapid elastic scattering rate. Additionally, neutrons with greater energy will—on average—lose more energy per scattering event. The neutron energy lost during an elastic scattering event is dependent on the atomic mass of the target nucleus and the scattering angle. The maximum neutron energy loss—corresponding to the minimum residual neutron energy (E'_{min})—due to an elastic scattering event is dependent on the atomic mass of the target nucleus is described by equation (1).

$$E'_{min} = (\frac{A-1}{A+1})^2 * E \quad (1)$$

The incident neutron energy is represented by E, A is the target nucleus atomic mass, and E'_{min} is the minimum energy of the scattered neutron. For neutron elastic scattering on Pb, this maximum neutron energy loss is approximately 1.9%.

The continuous elastic scattering of a large population of interrogation neutrons produced at the same time (t_0) results in a Gaussian distribution of neutron energy with an average energy ($\bar{E}$) which is a function of the time (t) after the initial pulse (t_0). This average neutron energy decreases with time until the subsequent pulse. The time-energy correlation of the LSDS can be characterized theoretically using four basic assumptions of the interrogation neutrons: (1) there is no neutron multiplication in the slowing-down medium, (2) inelastic scattering is absent, (3) elastic scattering is isotropic in the center of mass, and (4) the chemical binding and thermal motion effects are neglected [40]. Detailed Monte Carlo simulations and experimental measurements, which account for the aforementioned assumptions, can be used to verify the theoretical relationship between slowing-down time and energy and the corresponding LSDS energy resolution. The average neutron energy $(\bar{E})$ of the RPI LSDS was previously determined and is defined by equation (2), where $k \approx 165{,}000$ eVμs^2 and $t_0 \approx 0.3$μs for the RPI LSDS.

$$\bar{E} = \frac{k}{(t_0 + t)^2} \tag{2}$$

The energy resolution of a slowing-down spectrometer is heavily dependent on the atomic composition of the slowing-down medium and is specifically sensitive to hydrogen impurities. This energy resolution is time-dependent and becomes narrower as neutron diffusion continues. The energy resolution of the RPI LSDS was characterized to be about 35% (FWHM) in the energy range from 1 eV to 20 keV. The resolution of the LSDS as a function of the average neutron energy can be calculated using equation (3) [41]. Additionally, RPI LSDS resolution function is plotted in Figure 2.1.

$$\frac{\Delta E}{\bar{E}} = \sqrt{\frac{0.128}{\bar{E}} + 0.0835 + 3.05x10^{-5}\bar{E}} \tag{3}$$

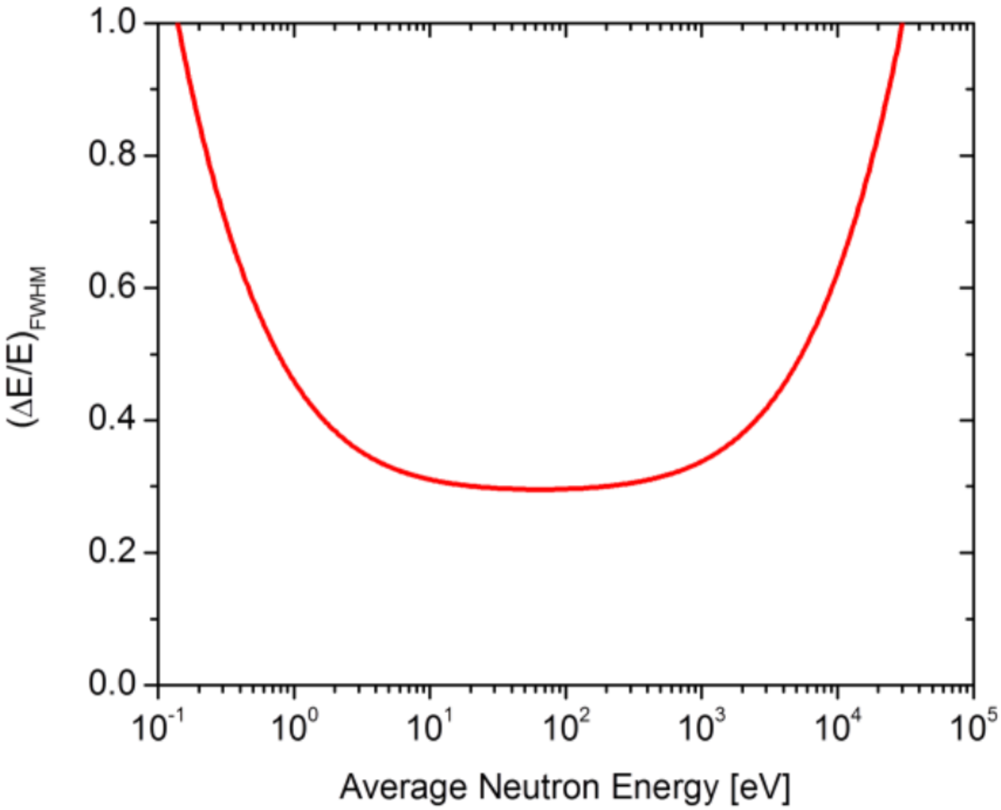

Figure 2.1: Full-width at half-maximum of the RPI LSDS as a function of average neutron energy

The spatial distribution and energy-dependent interactions of the interrogation neutrons are governed by the neutron transport equation, which is a function of time, space, energy, and direction. Complete and meticulous derivations of the theoretical neutron spatial distribution, mean energy, and resolution were previously performed for the RPI LSDS [9], [18].

2.1 Fissile Assay Using the RPI LSDS

Neutron cross-section measurements using LSDS require the knowledge of the LSDS time-energy correlation function, the sample mass, the isotopic composition, and the ability to detect and track neutron events with small time increments [39]. Alternatively, the LSDS can be used to determine a sample's isotopic mass, given that the cross-section data and LSDS resolution are well-known [17], [42]. The LSDS method for fissile assay was first proposed in the 1970's and is the basis for investigating the feasibility of employing the LSDS for SNF assay [38].

In simplistic terms, the methodology of applying slowing-down spectroscopy for fissile assay involves placing a fissile sample within the LSDS and continuously producing pulses of neutrons at the center of the spectrometer, which are used to interrogate the sample. The slowing-down interrogation neutrons can impinge on the sample, resulting in fission events. The fission rate produced within the sample, $R_f(E)$, is represented by equation (4), where Φ(E) is the energy-dependent neutron flux [n/cm^2-s], $\Sigma_f(E)$ is the energy-dependent macroscopic fission cross-section of the fissile material [cm^{-1}], and t is this effective neutron track length through the fissile sample [cm].

$$R_f(E) = \Phi(E) * \Sigma_f(E) * t \tag{4}$$

Fissions induced in the fissile sample by interrogation neutrons can be detected using threshold fission chambers. These fission chambers, which are referred to as assay chambers, utilize a fissionable material—e.g. ^{238}U or ^{232}Th—to discriminate high-energy fission neutrons from lower energy interrogation neutrons. The time-dependent response of these assay chambers is characteristic of the isotopic composition of fissile sample. This time-dependent response of the assay chambers is corresponds to the shape of the fissile sample's fission cross section, which is broadened by the LSDS resolution and convoluted by the time-depended neutron flux in the LSDS.

2.2 The RPI LSDS

At the RPI Gaerttner LINAC Center, an LSDS has been maintained and used for nuclear data measurements since the 1970's. A picture of the spectrometer can be seen by Figure 2.2. The fundamental components of the RPI LSDS system adapted for fissile assay are as follows [10]:

1. A 66 metric ton cube constructed from high-purity Pb bricks
2. A thermal neutron-absorbing Cd cover surrounding the Pb
3. An interrogation channel for fissile sample housing

4. An assembly box to contain the fissile samples and detectors
5. The RPI electron linear accelerator (LINAC) and an air-cooled tantalum (Ta) photoneutron target used as a pulsed neutron source
6. A ^{235}U fission chamber (flux monitor) used to normalize individual measurements to chances in the LINAC beam conditions.
7. Threshold fission chambers (assay chambers) used to discriminate fission neutrons from interrogation neutrons
8. Fission (probe) chambers lined with isotopic fissile material (^{235}U and ^{239}Pu) for implementation into a semi-empirical analysis algorithm
9. Backend electronics with the ability to discriminately measure the neutron signal as a function of slowing-down time

Figure 2.2: Picture of the LINAC beam tube entering the RPI LSDS

The LSDS at RPI is a 1.8 m cube of high-purity Pb weighing about 66 metric tons. The faces of the LSDS are covered with a 0.75 mm-thick sheet of Cd, which prevents thermal neutrons from re-entering the LSDS. There is an interrogation channel (15cm x 15cm) through the Pb; one end is closed and the other covered with neutron absorbers, e.g. Cd or boron (B) plates. An aluminum (Al) housing, which lies in the interrogation channel, is used to hold the fissile samples and assay detectors. Additionally, there are assay detectors centrally-fix in the Pb directly above the fissile samples within the aluminum housing. In the upper corners of the Pb are small ports for external flux monitors used to normalize independent experiments to standard beam conditions. The electron beam travels into the center of the Pb, where it is incident on the Ta neutron target. The Ta photoneutron target is composed of 11 Ta plates with three different thicknesses. The plates are separated by 1.5mm and compose of a 5cm cube. The target is cooled with air, and the temperatures of the target and surrounding Pb are monitored to prevent melting. A representation of the RPI LSDS is provided by Figure 2.3.

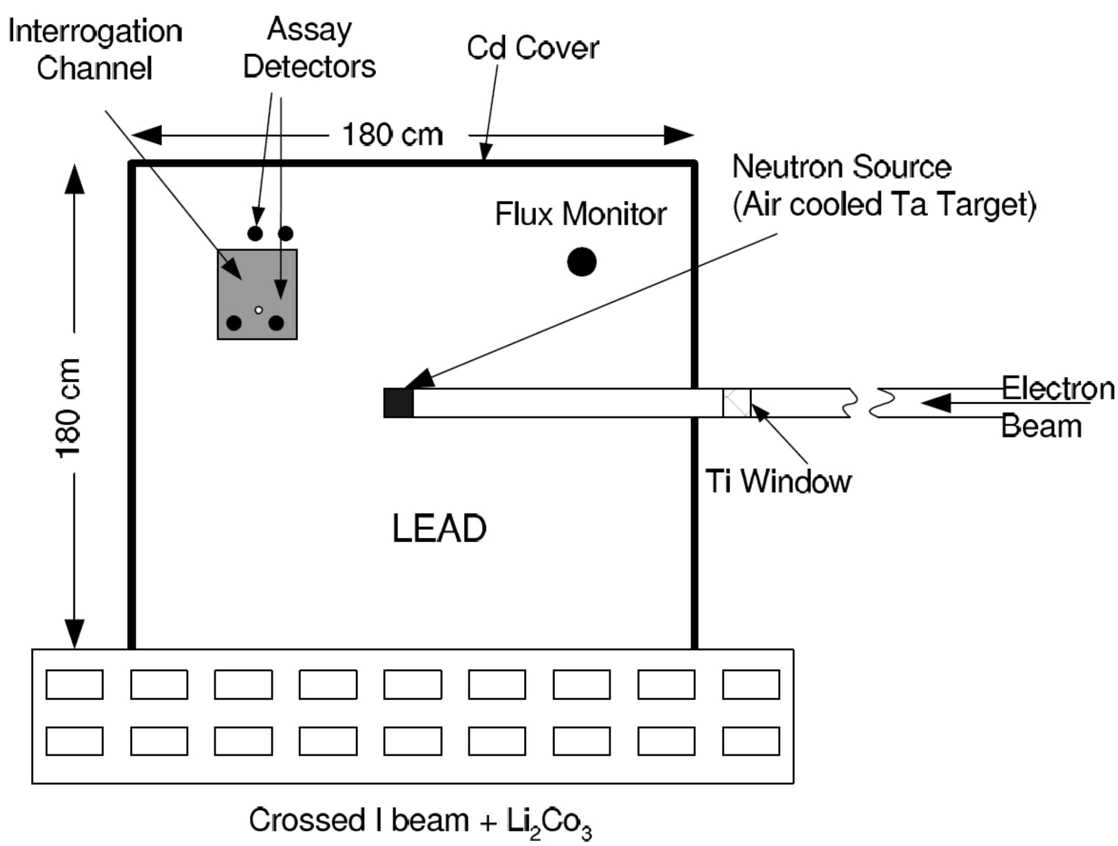

Figure 2.3: (Side view) Diagram of the LSDS at Rensselaer Polytechnic Institute's Gaerttner LINAC Center

2.3 The RPI LINAC

The requirements of a neutron source for the application of fissile assay using an LSDS are as follows [17]:

1. The neutron source must be pulsed and repetitious with a pulse width < 1μs wide and frequency of 180 Hz.
2. Each pulse must produce a large neutron flux; typical RPI beam conditions and a frequency of 180 Hz result in ~$3x10^{12}$ n/s. Less intense neutron pulses will reduce the signal-to-noise ratio or the interrogation time.
3. The initial neutron energy must be on the order of 1 MeV.

The Gaerttner LINAC Laboratory at RPI (depicted in Figure 2.4) began operation in December of 1961, and was designed to perform neutron TOF measurements for the purpose of improving nuclear data libraries for various neutron reactions [35]. Additionally, a new 40m station was built but is not depicted in Figure 2.4. This LINAC is used to produce intense pulses of neutrons for TOF and slowing-down spectroscopy experiments. Experimentally, the LINAC pulsed neutron source is the most significant component of the nuclear data capabilities at RPI, allowing for cross-section measurements to be performed with low statistical uncertainty over a broad energy range.

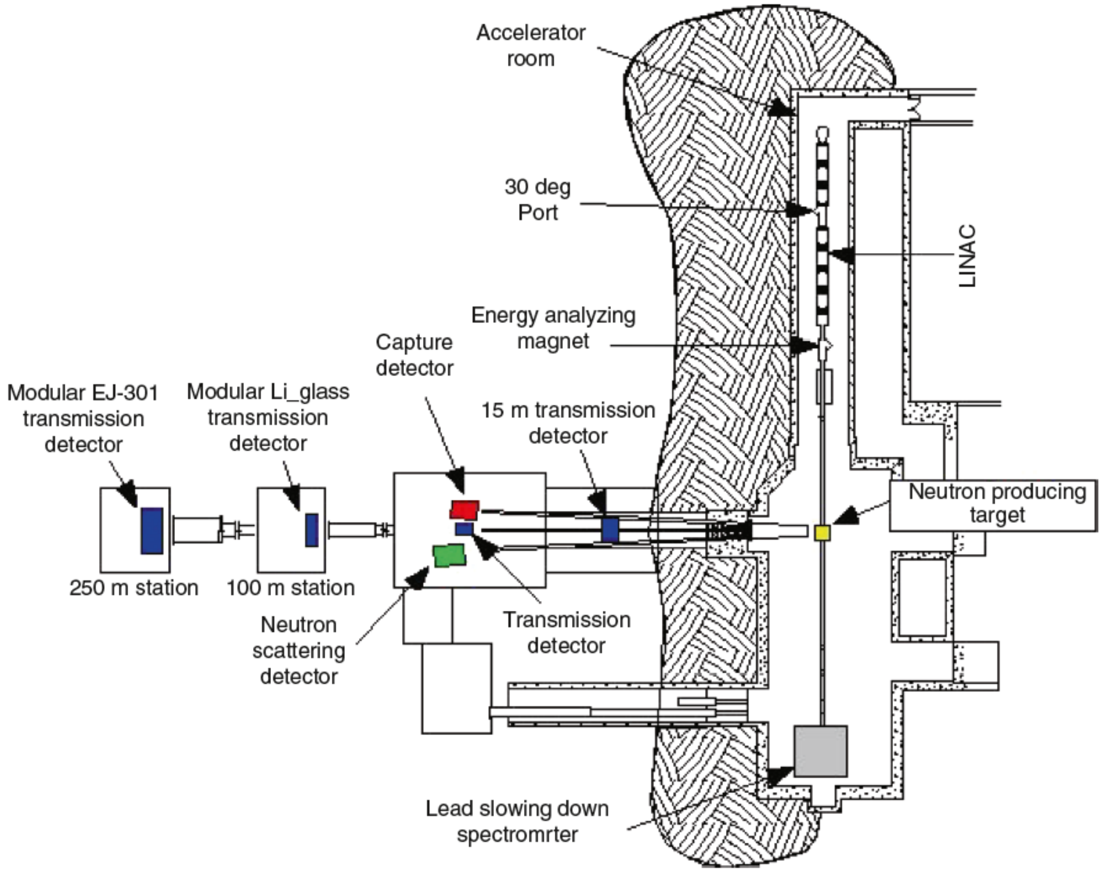

Figure 2.4: Layout of the RPI LINAC and detector stations

For assay experiments with the LSDS, the TOF photoneutron target is removed, and the electron beam is guided to the LSDS target at the center of the lead pile. The accelerator is tuned to a pulse frequency of 180 Hz, an electron current of 10-15μA, and electron energy of ~50 MeV. The electrons from the LINAC interact with the air-cooled Ta target and produce gammas via Bremsstrahlung radiation, shown in equation (5).

$$e + Ta \rightarrow \gamma \tag{5}$$

These γ's interact in subsequent layers of Ta, producing photoneutrons.

$$\gamma + Ta \rightarrow n \tag{6}$$

Approximately 0.03 neutrons are produced per incident electron, which results in a neutron intensity is $1.5x10^{10}$ neutrons/pulse. Therefore, a typical 60 minute experiment with the aforementioned beam conditions produces about $1x10^{16}$ neutrons [9], [41]. The energy spectrum of these neutrons can be represented by an evaporation spectrum with an average neutron energy of 0.46 MeV, expressed mathematically by equation (7), where E is the neutron energy expressed in MeV [9].

$$\phi(E) \sim E * \exp(-\frac{E}{0.46}) \tag{7}$$

The evaporation spectrum of the pulsed neutron source can be seen by Figure 2.5.

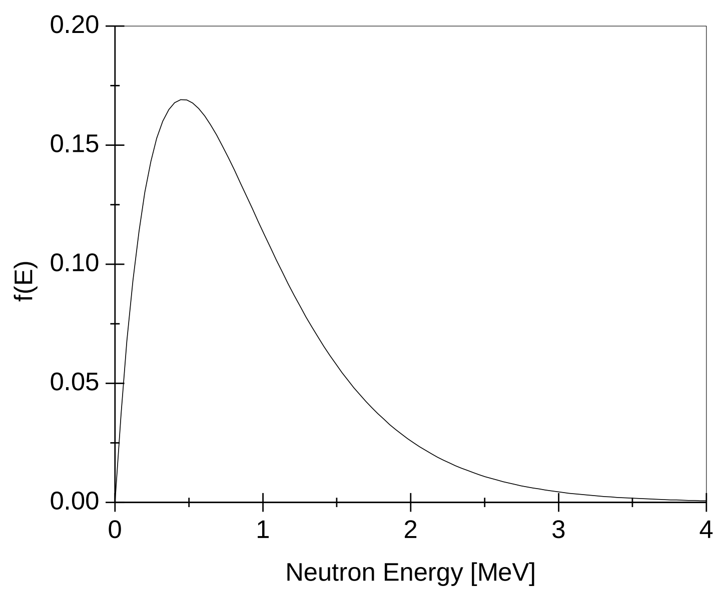

Figure 2.5: The evaporation spectrum of the Ta photoneutron target with a neutron temperature of 0.46 MeV

3. MONTE CARLO SIMULATION OF THE LSDS

Monte Carlo N-Particle Transport Code Extended (MCNPx) [43] was used to simulate the individual assay experiments performed with the RPI LSDS. These simulations were compared to experimental results in order to verify the interpretation of the results.

3.1 Lead Impurity Analysis

The isotopic composition of the slowing-down medium has a significant impact on the resolution and time-energy correlation of the interrogation neutrons. Therefore, while the Pb composing the LSDS is high-purity (99.99%), the residual isotopic impurities must be incorporated in the MCNPx simulations of the LSDS configuration. While hydrogen impurities result in the greatest deficiency of the LSDS resolution due to their atomic mass of one, other isotopic impurities found in quantities on the order of parts per million (ppm) can impact the performance of the LSDS. Therefore, two chemical analyses of the LSDS's Pb were performed in order to quantify these impurity levels.

An original analysis of the Pb was performed in 1971 via emission spectroscopy by Knolls Atomic Power Laboratory (KAPL) [9]. A more recent analysis by Korea Atomic Energy Research Institute (KAERI) in February 2012 provided a more accurate set of impurities, including a value for the hydrogen content. Table 3.1 displays the results of both Pb analyses.

Table 3.1: Comparison of two Pb impurity analyses performed on samples of the LSDS

Impurity	Weight Fraction (μg/g)	
	1971 KAPL E.S. Analysis	2012 KAERI Analysis
C	-	20
H	-	1.0
Ag	1.8	1.31
B	-	0
Cu	0.8	4.52
As	<25	0.04
Sb	<2	0.11
Ni	<10	0.15
Zn	-	0.03
Cd	-	0.01
Fe	<20	1
Sn	1	0.03
Te	-	0.19
Gd	-	0.01
Sm	-	0.01
Tl	-	2.54
Bi	45	11.53

Monte Carlo simulations were performed with three Pb compositions, corresponding to pure, natural Pb and the two individual impurity analyses. The effect of the isotopic impurities is most noticeable in the thermal region, so a fissile probe chamber was used for this investigation. Specifically, the experimental response of ^{235}U flux monitor located in the assembly box in the absence of additional fissile material was compared to a corresponding MCNPx simulation. The internal ^{235}U fission chamber was simulated using an F5 flux tally, which was convoluted with a ^{235}U tally multiplier (FM) card. The tally was collected as a function of slowing-down time. Neutron cross-sections were called using ENDF/B-VII.0. The neutron source was simulated at the center of the lead with the evaporation neutron spectrum described in equation (7). The simulations were performed until adequate counting statistics in each time window were collected. These simulations were plotted and compared to an experimental background measurement in order to demonstrate the effect of impurities on the slowing-down behavior of the LSDS. Figure 3.1 shows the ^{235}U detector response as a function of slowing-down time from 0 to 4.0 ms. The MCNP simulations were normalized to the integrated experimental detector response from 1 to 100μs, which represents the ^{235}U resonance region. Figure 3.2 exhibits the same responses, but the plot is focused on the region most significantly affected by impurities in the Pb (>200μs).

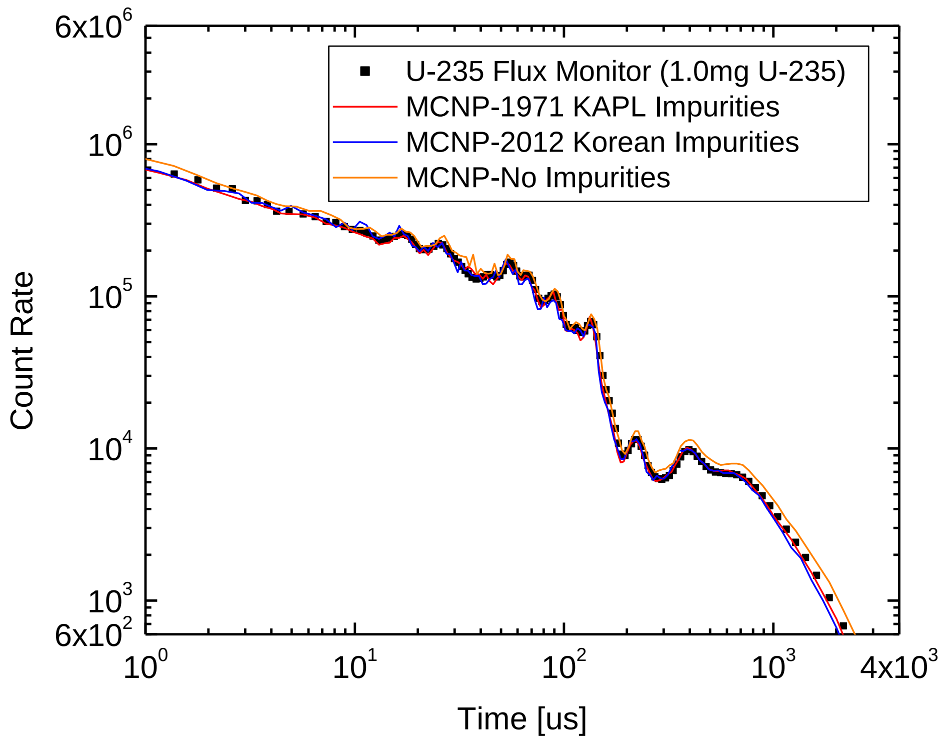

Figure 3.1: Simulated ^{235}U detector responses corresponding to the Pb impurity analyses, compared with the experimentally **measured response**

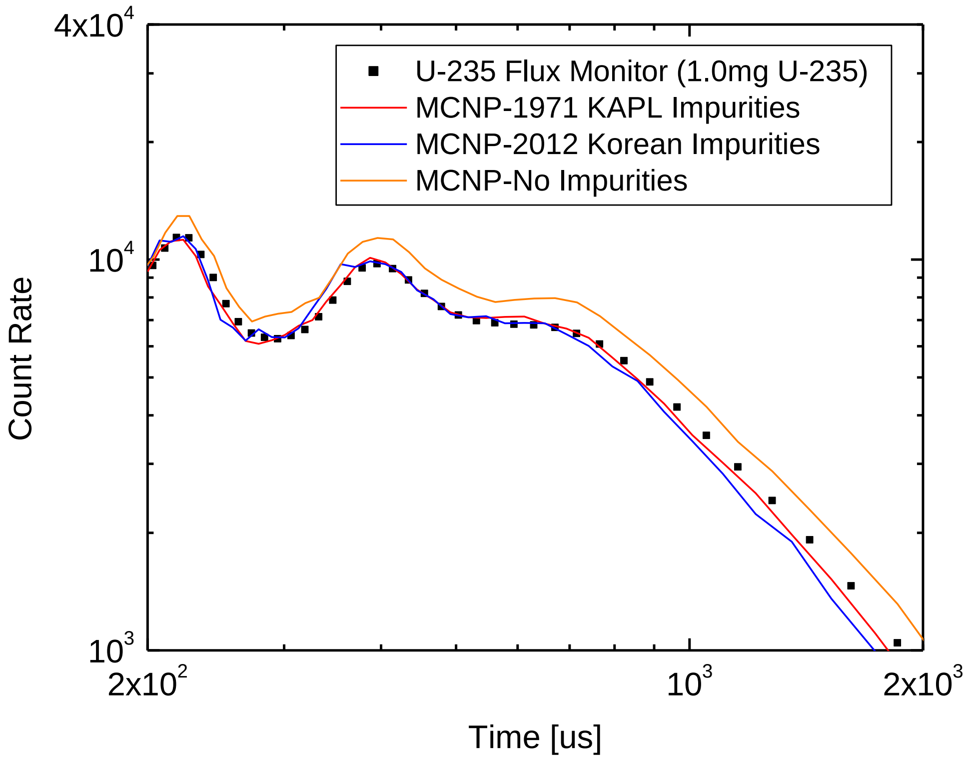

Figure 3.2: Response from Figure 3.1, focused on the thermal region to demonstrate the impurity effect on neutron absorption and resolution broadening

The slight spectral shift and reduced thermal peak seen in the simulation with pure Pb demonstrate that the impurities in the Pb both broaden the energy resolution of the LSDS and cause neutron absorption. The disagreement between the experimental response and simulated tally of the internal ^{235}U fission chamber in low energy region (t>200μs) corresponding to a pure Pb slowing-down medium suggests that impurities in the Pb are causing significant neutron absorption. This idea is reinforced by the improved agreement between the Monte Carlo simulations and the experimental detector response when the Pb impurities are accounted for. This improved agreement reinforces the importance of accurately modeling the material composition of the LSDS when using Monte Carlo simulations to benchmark experimental results.

3.2 Simulation Fissile Assay Experiments

The ^{235}U in SNF is residual fissile material from fresh fuel; however, the fissile plutonium—^{239}Pu and ^{241}Pu—is not present in unused fuel. Instead, neutron capture in ^{238}U and the subsequent decay of ^{239}U and ^{239}Np leads to the accumulation of ^{239}Pu. Successive neutron absorption in ^{239}Pu results in ^{240}Pu and ^{241}Pu buildup. Therefore, the fissile composition of used fuel from a particular reactor is a complex function of the initial U enrichment, burnup, and cool-down time. Moreover, the composition of individual pins within a SNF assembly will vary depending on their radial position inside the assembly during reactor operation.

The principle of LSDS for the assay of fissile materials is that the shape of the assay detector responses will be a function of the relative abundance of the three fissile isotopes of interest—^{235}U, ^{239}Pu, and ^{241}Pu. Each of the aforementioned isotopes found in SNF has a unique energy-dependent fission cross-section with distinct resonances. Characteristics of these cross-sections can be seen by the time-dependent fission neutron production, which is measured by the assay chambers.

The simulation of a hypothetical assay experiment with a four faux fuel pins within the RPI LSDS was performed in order to illustrate the individual contribution of four isotopes (^{235}U, ^{238}U, ^{239}Pu, ^{240}Pu, and ^{241}Pu) to the total fission signature. ^{238}U and ^{240}Pu were included in this investigation because of their neutron absorbing properties. The composition of the four simulated fuel pins is shown in Table 3.2.

Table 3.2: Relative isotopic compositions of four hypothetical fuel pins used to demonstrate the individual time-dependent fission responses of three fissile isotopes during interrogation within the LSDS

Fuel Pin	^{235}U [%]	^{238}U [%]	^{239}Pu [%]	^{240}Pu [%]	^{241}Pu [%]
1	-	96	-	-	4
2	-	96	4	-	-
3	-	-	4	96	-
4	4	96	-	-	-

Figure 3.3 depicts the response of a ^{238}U assay chamber as a function of slowing-down time for each of the four fictitious fuel pins. The detector was tallied with an F4 tally (average flux within a cell) convoluted with the ^{238}U fission cross-section. The relative compositions of the aforementioned fuel pins are listed in the legend, and the contributions of individual isotopic resonances to the aggregate assay responses are labeled in Figure 3.3.

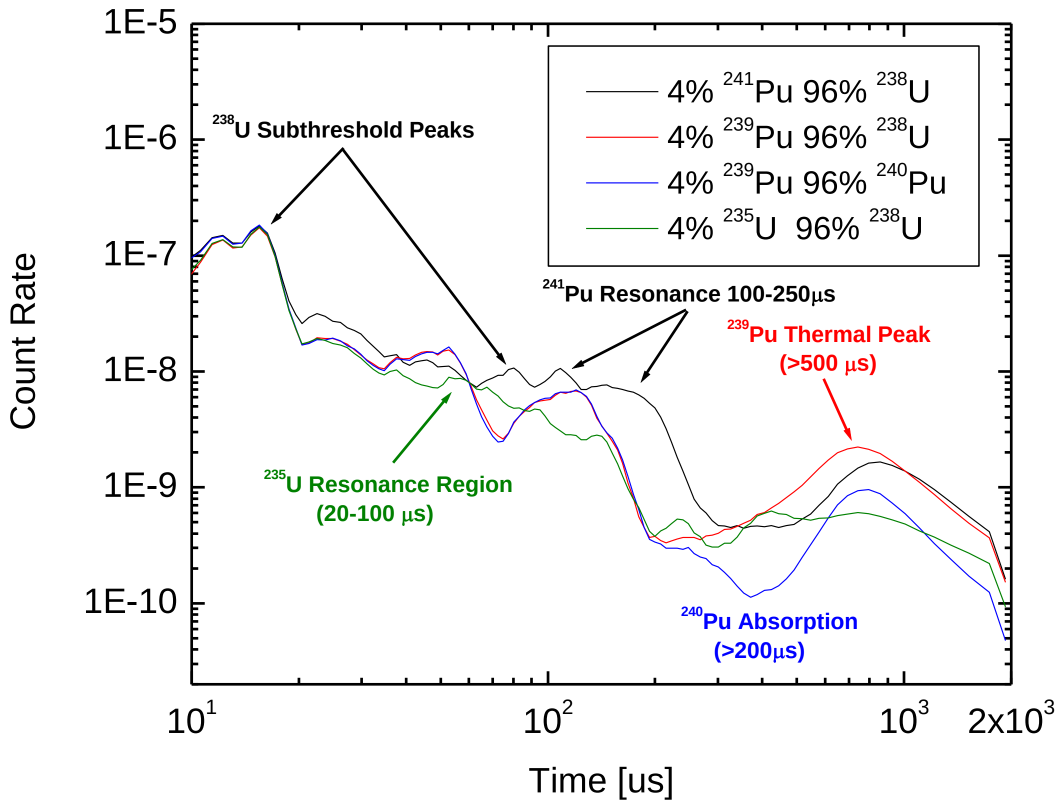

Figure 3.3: MCNPx simulations demonstrating the unique fission and absorption structure of ^{235}U, ^{239}Pu, ^{240}Pu, and ^{241}Pu when interrogated in the LSDS

3.3 NGSI-64 Fuel Assemblies

The Next Generation Safeguards Initiative (NGSI)—launched by the National Nuclear Security Administration (NNSA)—has determined the complete composition of a library of fuel assemblies using computer codes to simulate fuel burnup. NGSI provides the composition of each individual fuel pin composing a 17x17 SNF assemblies corresponding to 64 assemblies with various initial enrichment, burnup, and cool-down time. These assemblies ranged from an initial enrichment of 2-5%, a burnup of 15-60 gigawatt-days per metric ton uranium (GWD/MTU), and a cool-down time of 1-80 years [44]. These 64 modeled assemblies—along with 27 diversion assemblies—were used to create MCNP input files corresponding to various SNF assemblies. The simulation of these assemblies within an LSDS was used to evaluate the mathematical models used to quantify the fissile mass of interrogated SNF assemblies [42].

MCNP simulations of individual fuel pins within the interrogation channel of the RPI LSDS were performed. The five simulated fuel pins had an initial enrichment of 4.0% ^{235}U, an incremental burnup—varying from 0 to 60 MWD/MTU—and a cool-down of 1 year. The resulting simulation of the assay chamber response is shown in Figure 3.4. The detailed isotopic composition of each fuel pin is provided in Table 3.3. The assay chamber response corresponding to the interrogation of each fuel pin was simulated using an F5 tally convoluted with the ^{238}U fission detector. Figure 3.4 demonstrates how the time-dependent assay response changes as a function of fuel burnup, and illustrates the sensitivity of the RPI LSDS to incremental fissile material for the application of a single fuel pin assay. These simulations demonstrate the ability use LSDS to assay SNF samples.

Table 3.3: U and Pu composition of NGSI fuel pin corresponding to Figure 3.4

Burnup (GWD/MTU)	^{238}U Mass (g)	^{235}U Mass (g)	^{239}Pu Mass (g)	^{241}Pu Mass (g)
Fresh	700.9	24.2	0	0
15	695.1	18.2	2.85	0.27
30	687	10.5	3.58	0.72
45	678.2	5.4	3.68	1.02
60	668.8	2.5	3.62	1.14

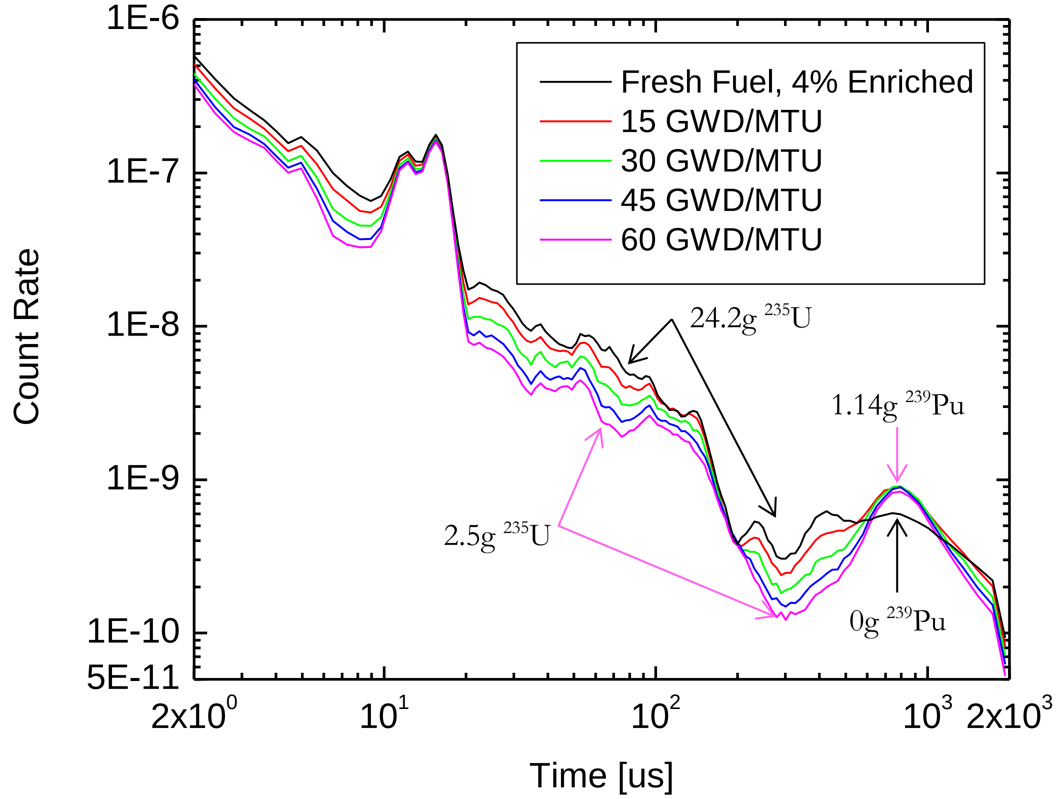

Figure 3.4: Simulated assay of various individual fuel pins from the NGSI in the RPI LSDS

4. EXPERIMENTAL SETUP AND MEASUREMENTS

Experiments were performed at the Gaerttner LINAC Center at RPI throughout August and September of 2012 with the objective of benchmarking the RPI LSDS for the assay of fissile Pu and U. These experiments involved the use of samples containing fissile U and Pu, multiple assay chambers, and a flux monitor. The fissile samples utilized in these experiments, along with the assay detectors, were situated in an aluminum assembly box within the interrogation channel of the LSDS. Additionally, an internal ^{235}U and ^{239}Pu fission chamber were placed in this assemble, the responses of which were collected for implementation in the PNNL assay algorithm. A drawing of the new assembly faceplates which housed the samples and detectors can be seen in Figure 4.1. Figure 4.1 also shows numerical labels corresponding to each of the assembly box's holes, which were used to denote the location of individual samples and detectors. The displayed units are centimeters. The original Al assembly box, pictured in Figure 4.2, was centered in the interrogation channel. One end of the channel is closed with Pb bricks, and the other was covered with neutron absorbing Cd and B. A picture of the assembly box inside of the LSDS interrogation channel with four fission chambers (two assay chambers and two smaller probe chambers containing ^{235}U and ^{239}Pu) can be seen in Figure 4.3.

Portions of this chapter previously appeared as: G. A. Warren et al., "Lead Slowing-Down Spectrometry Analysis of Data from Measurements on Nuclear Fuel," *Nucl. Sci. and Eng.,* vol. 179, no 3., pp. 1-10, Mar. 2015.

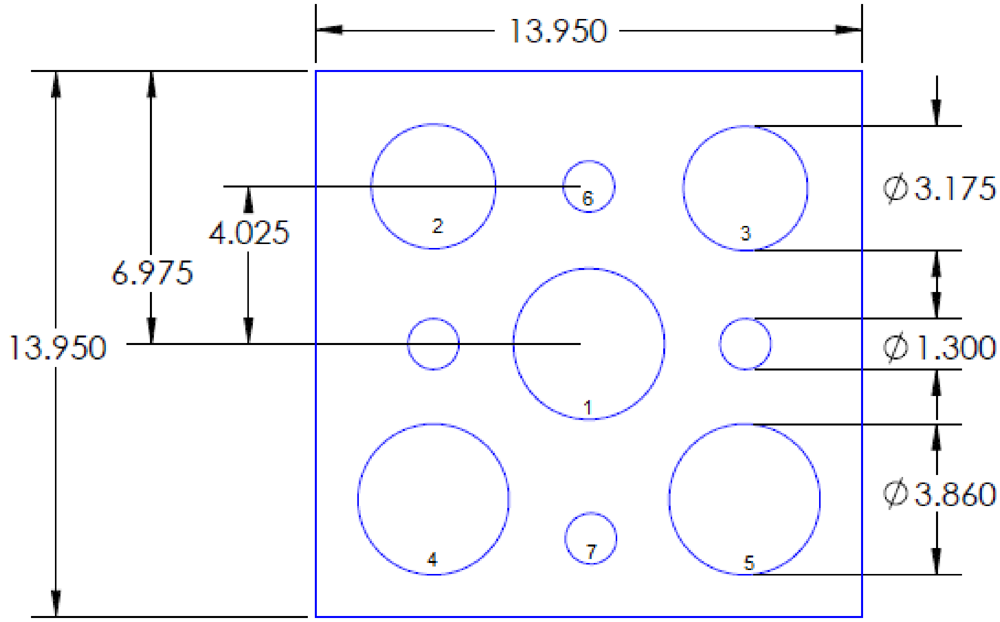

Figure 4.1: Drawing of the new Al faceplate used to hold the detectors and samples with units of cm

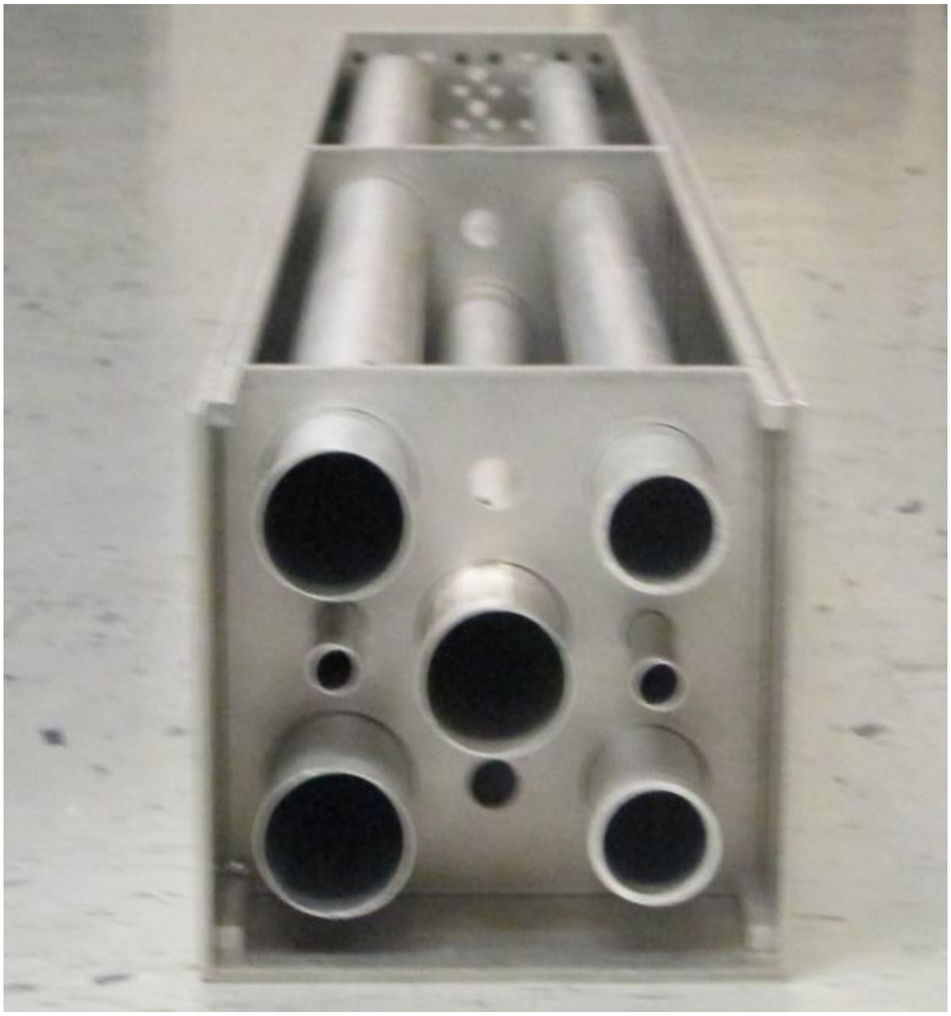

Figure 4.2: New Al assembly box used to house fissile samples, assay detectors, and isotopic fission chambers for the benchmark experiments in the RPI LSDS

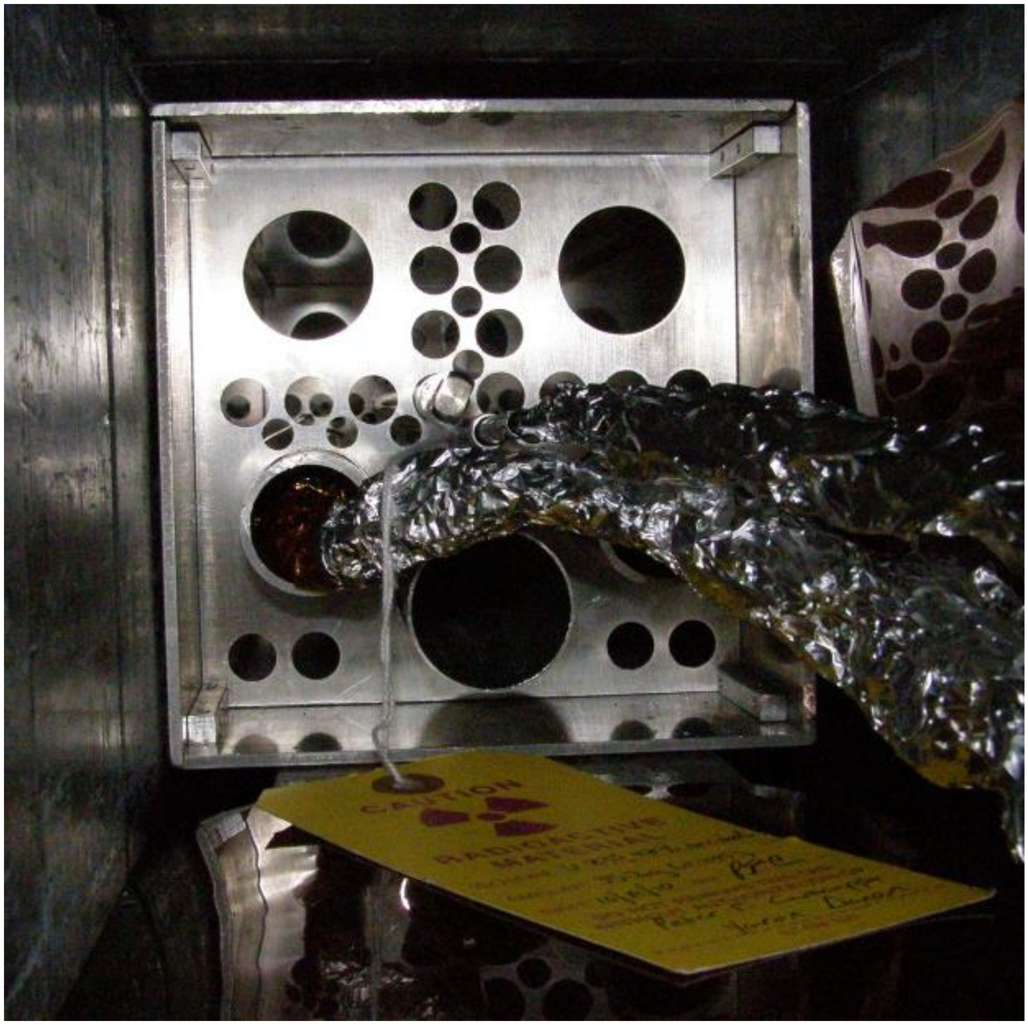

Figure 4.3: Picture of the original Al assembly box inside of the LSDS interrogation channel with four fission chambers

4.1 Fissile Samples

Due to the high cost of handling and transporting SNF, experiments at the Gaerttner LINAC Center were performed with a variety of fissile samples, including: a fresh special power excursion reactor test (SPERT) fuel pin from the RPI Walthousen Criticality Facility, two Plutonium-beryllium (PuBe) neutron sources, and ten highly enriched uranium (HEU) disks (93.3% ^{235}U). Each disk has an approximate diameter of 1.27cm and contained between 200 and 300mg of ^{235}U. A description and the position—corresponding to the labels in Figure 4.1—of these fissile samples are shown in Table 4.1. Detailed information about the SPERT fuel pin and Pu sources can be found in the SNM license in Appendix A.

Table 4.1: Fissile specimens assayed in recent RPI LSDS experiments

Sample	Isotope	Isotopic Mass [g]	Location in Assembly
SPERT Fuel Pin	^{235}U	34.8 ± 0.2	1
Large ^{239}PuBe Source	^{239}Pu	91 ± 5	4
Small ^{239}PuBe Source	^{239}Pu	47 ± 2	5
HEU Disks(1-5)	^{235}U	1.290 ± 0.006	1
HEU Disks (1-10)	^{235}U	2.631 ± 0.009	1

The fresh SPERT fuel pin has an enrichment of 4.8 w% (4.866 at%), containing 34.8 g of ^{235}U and 689 g of ^{238}U. The fuel region of the pin has a length of 91.4 cm, diameter of 1.07 cm, and the cladding is stainless steel with a thickness of 0.05 cm. The large PuBe source has an outer diameter of 3.6 cm, a length of 8.3 cm, and contains 91g of ^{239}Pu. The small PuBe source has an outer diameter of 2.5 cm, a length of 6.6 cm, and contains 47g of ^{239}Pu. The ten HEU disks—enriched to 93%—have an approximate diameter of 1.3 cm. Each disk contains between 0.2 and 0.3g of ^{235}U. The individual masses of the HEU disks can be seen in Table 4.2.

Table 4.2: Elemental and isotopic (^{235}U) masses corresponding to each of the 10 disks (93% ^{235}U)

Disk Number	Uranium Mass [g]	^{235}U Mass
1	0.2631±0.0003	0.2446±0.0003
2	0.2708±0.0003	0.2518±0.0003
3	0.2545±0.0003	0.2367±0.0003
4	0.2528±0.0003	0.2351±0.0003
5	0.2489±0.0003	0.2315±0.0003
6	0.2477±0.0003	0.2303±0.0003
7	0.3046±0.0003	0.2833±0.0003
8	0.2613±0.0003	0.2430±0.0003
9	0.2518±0.0003	0.2342±0.0003
10	0.2756±0.0003	0.2563±0.0003

4.2 Neutron Detection Systems

As previously mentioned, the assay chambers used to detect the fission signal induced in the fissile samples by the interrogation neutrons contain ^{232}Th and ^{238}U. These detectors were manufactured by Westinghouse with an active length of 20 cm and a diameter of 2.5 cm [10]. Each contains about 200 mg of fissionable material was operated with a bias voltage of +300 V. The ^{238}U assay chamber contains highly depleted U, with a residual ^{235}U composition of 4.1 ppm. This level of U depletion is required to reduce the response from residual ^{235}U. The rarity of this depleted U makes these detectors irreplaceable. The ^{232}Th detector contains even less fissile material (<25 ppb ^{235}U), which leads to a better noise ratio; however, the relatively small ^{232}Th fission cross-section makes the ^{238}U about three times as efficient [45].

The relative neutron flux produced by the LINAC was monitored with a ^{235}U fission chamber, located in the upper corner of the RPI LSDS (shown in Figure 2.3). This flux monitor contains 1.0 mg of fissile ^{235}U. Since the LINAC beam conditions can vary during individual experiments, this detector was used to normalize the assay detector responses to a constant neutron flux in the spectrometer. Two additional small fission chambers (^{235}U and ^{239}Pu) were positioned in the assembly box for the use in the semi-empirical assay algorithm developed at PNNL [42]. The content and position of the four detectors within the assembly box (Figure 4.1) are shown in Table 4.3.

Table 4.3: Fission chamber detectors positioned in RPI LSDS assembly box

Detector	Nominal Mass [mg]	Location in Assembly
^{238}U Assay Detector (Pb)	200	Above Interrogation Channel
^{238}U Assay Detector	200	2
^{232}Th Assay Detector	200	3
^{235}U Flux Monitor	1.0	6
^{239}Pu Flux Monitor	0.3	7

4.2.1 Detector Electronics

The signal corresponding to the aforementioned fission chamber detectors first requires preamplification, which is performed by a modified Cremat CR-110 preamplifier with a time constant of 45ns (R=15kΩ and C=3pf). Next, a Cremat Gaussian shaping amplifier was used to shape the pulse with an integration time of 100ns. The shaped pulse was input into an ORTEC CF 8000 constant fraction discriminator, which was used to discriminate fission events from background alpha particles from the decay of the fission chamber contents (e.g. ^{235}U, ^{232}Th, etc.). The discriminator thresholds were determined by exposing the detector to a neutron source and collecting a pulse height spectrum. A pulse height spectrum is a histogram of the individual pulse heights and is collected using a multichannel analyzer (MCA) and the related software. An example of a neutron-induced ^{235}U fission chamber pulse height spectrum without a discriminator can be seen by the black response in Figure 4.4. The red pulse height spectrum in Figure 4.4 was collected with a discriminator of -181 mV in coincidence. The discriminator effectively rejects the aforementioned alpha pulses, while counting the fission events.

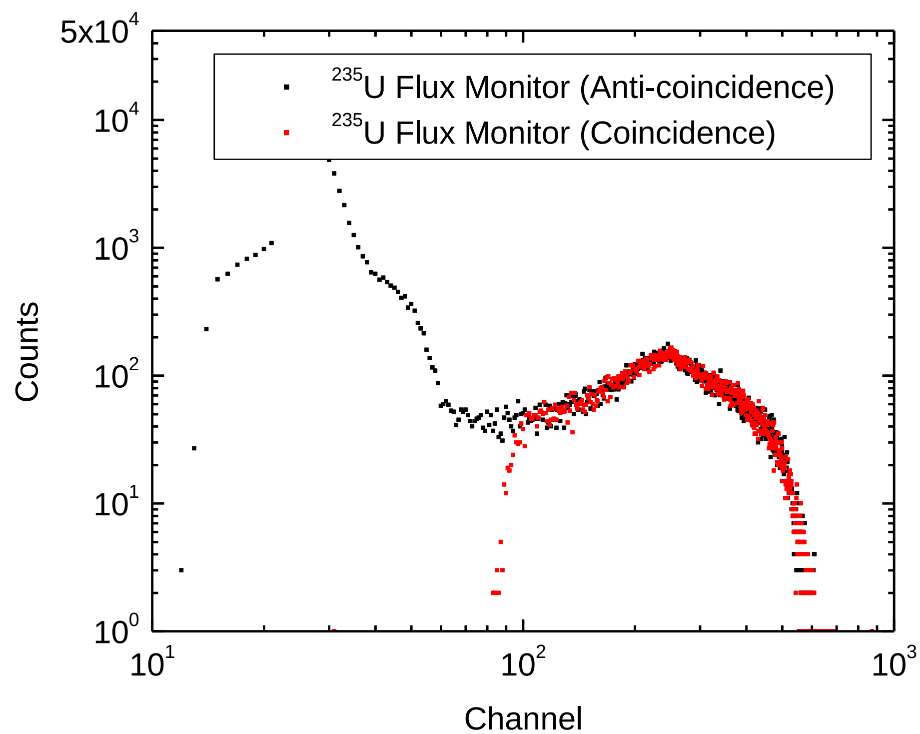

Figure 4.4: ^{235}U flux monitor response with and without the calibrated discriminator set to -187.4 mV

A Time-of-flight clock (FAST ComTec MCS6) was used to collect the fission chambers responses as a function of slowing-down time. This particular TOF clock was set to have discrete time bins of 409.6 ns. Each time the LINAC pulse is incident on the LSDS target, there is a delay of several μs before the gamma flash. The t_0 signal is set to this gamma flash, which was input into the clock's start channel. Each t_0 signal triggered the clock to begin a sweep, creating a time-dependent response for each fission chamber. These responses were corrected for the detector dead time, adjusted for the t_0 delay (0.3μs), and grouped into larger time bins. The diagram of the aforementioned electronics and data acquisition system for a single detector is depicted by the diagram in Figure 4.5.

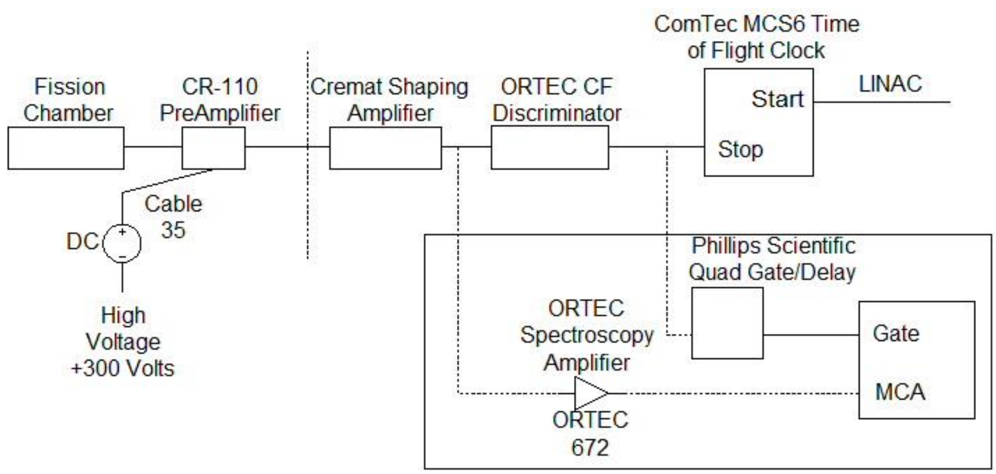

Figure 4.5: Diagram of the neutron detection and data acquisition systems used to collect the time-dependent neutron response with the ^{235}U fission chamber

4.3 Experimental Configurations

The experiments at RPI were performed with variable quantities of fissile Pu in the presence of variable ^{235}U. This investigation required numerous experimental arrangements, which were altered between LINAC runs. At the start of each day, a 60-minute background measurement was performed. Each subsequent experiment involved 30 minutes of data collection (or 324,000 LINAC pulses), with enough cool-down time between experiments to allow for the decay of background radiation to a safe level. The various experimental setups utilized combinations of the SPERT fuel pin, 10 HEU disks, and the small and large PuBe sources. Each measurement was performed with the samples and detectors centered in the interrogation channel. A description of the experimental arrangements can be seen in Table 4.4.

Table 4.4: Descriptions of experimental measurements with the RPI LSDS

Trial	Fuel Pin	HEU disks	PuBe Source	Time (minutes)	Description
1	-	-	-	60	Background
2	-	-	Large	30	Large PuBe
3	-	-	Small	30	Small PuBe
4	-	-	Small + Large	30	Both PuBe
5	Yes	1-10	-	30	Pin + Disks 1-10
6	Yes	1-10	Large	30	Pin + Disks 1-10 + Large PuBe
7	Yes	1-10	Small + Large	30	Pin + Disks 1-10 + Both PuBe
8	Yes	1-10	Small	30	Pin + Disks 1-10 + Small PuBe
9	Yes	1-5	Large	30	Pin + Disks 1-5 + Large PuBe
10	Yes	1-5	Small	30	Pin + Disks 1-5 + Small PuBe
11	Yes	1-5	Small + Large	30	Pin + Disks 1-5 + Both PuBe
12	Yes	1-5	-	30	Pin + Disks 1-5
13	Yes	-	-	30	Pin
14	Yes	-	Large	30	Pin + Large PuBe
15	Yes	-	Small + Large	30	Pin + Both PuBe
16	Yes	-	Small	30	Pin + Small PuBe

4.3.1 Experimental Uncertainty

The uncertainty of the assay measurements can be divided into two categories: statistical uncertainty and systematic error. Statistical uncertainty can be improved by collecting more data, i.e. running longer experiments. It was previously determined that approximately 30 minutes of data collection for each experiment would provide adequate statistical uncertainty for subsequent data analysis [46].

Systematic uncertainty, on the other hand, is difficult to quantify. This type of uncertainty associated with the LSDS assay method arises due to fluctuations in the LINAC beam conditions, detector dead times, and positioning of the assay detectors and fissile samples.

As mentioned previously, variable beam conditions can be overcome by employing an external flux monitor to normalize individual experiments. Additionally, the detector dead-times remained <5% for the entire slow-down timeframe and dropped to below 2% after 50μs. Therefore, the detector dead-time corrections result in a relative uncertainty <1% [9]. Lastly, the uncertainty of the detector and sample positions are of concern since changes in these positions can result in significant fluctuations in the assay chamber responses. Therefore, the positions of each detector and fissile sample were measured carefully. Once the detectors and samples were positioned, they were secured and marked in order to limit this systematic uncertainty. Overall, the systematic uncertainty of the RPI LSDS assay methods was determined to be <2% [9].

4.4 Experimental Results and Analysis

The aforementioned experiments were performed at the RPI Gaerttner LINAC Center in August and September 2012. Two ^{238}U fission chambers (one in the assembly and another in the Pb above the interrogation channel) and one ^{232}Th fission chamber were employed as assay chambers. Throughout the experimental runs, the ^{238}U assay detector in the Pb above the interrogation channel performed most consistently. Throughout the experiments, the ^{235}U flux monitor was stationary in the upper-right corner of the LSDS. A second ^{238}U assay chamber, along with the fissile samples, one ^{235}U, and one ^{239}Pu fission chamber were secured in the center of the aluminum assembly box.

4.4.1 Experimental Benchmarking with MCNP Simulation

The preliminary benchmarking of the LSDS was performed by comparing the experimental results to Monte Carlo simulations. For instance, the experimental response of the ^{238}U detector corresponding to a single SPERT fuel pin sample was compared to a Monte Carlo simulation with the same configuration. This comparison can be seen in Figure 4.6. The experiment and simulation were normalized using the region from 40μs to 200μs and demonstrate good agreement above t=20μs. It is worth noting that the major discrepancy below 20μs arises because of deficiencies with ^{238}U sub-threshold fission cross-sections. Therefore, the MCNPx simulations—which can call specific cross-section libraries—do not agree with experiments in this region. The disagreement of ^{238}U subthreshold fission corresponding to two data libraries called by the simulation (formatted from ENDF/B-VII.0 and JEFF-3.1) can be seen in Figure 4.6. Since these discrepancies are only significant below 20μs, the ^{238}U assay chamber responses can still be used for assay above 20μs. ENDF/B-VII.0 was the library utilized for all subsequent simulations.

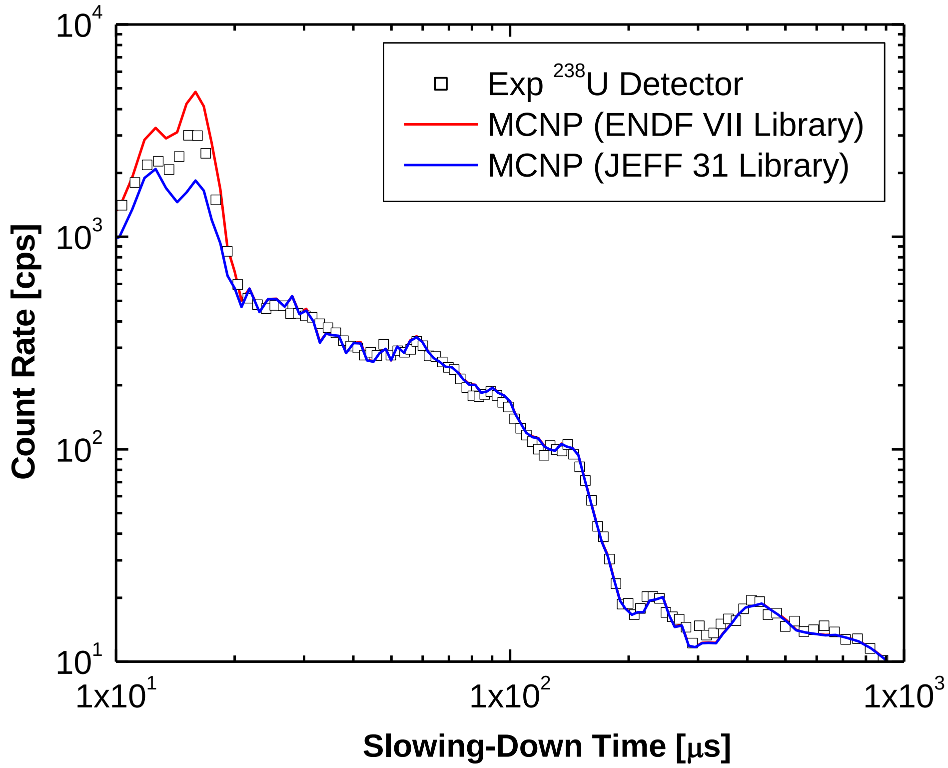

Figure 4.6: Experimental and simulated responses of the ^{238}U detector (Pb) with a SPERT fuel pin sample comparing ENDF/B-VII.0 to JEFF-3.1

4.4.2 Assay of Incremental Fissile Material

The small and large Pu samples (PuBe sources) were incrementally interrogated in order to assess the behavior of the assay detectors in response to large increments of Pu. Since these Pu samples contain large quantities of ^{239}Pu (47g and 91g, respectively), significant differences in the magnitude of the assay chamber's responses are expected. The responses of the ^{238}U assay detector in the Pb corresponding to these large increments of Pu mass were normalized using the flux monitor and are illustrated by the left-hand side of Figure 4.7. As expected, there is a clear difference in the magnitude of the responses corresponding to these four initial measurements. The normalized and dead time-corrected responses of Figure 4.7 (left) were integrated over a slowing-down region of 40 to 200μs. The right-hand side of Figure 4.7 shows the relative increase of the normalized and integrated count rates in this slowing-down region as a function of the added ^{239}Pu mass. The error bars represent the statistical uncertainty of the integrated measurements.

4.4.2.1 Self-Shielding Considerations

The right-hand-side of Figure 4.7 plot demonstrates a linear relationship between the relative count rate and the added ^{239}Pu mass. However, since the two Pu samples assayed for this measurement are large and contain a considerable amount of ^{239}Pu there are self-shielding effects in the samples. This arises because interrogation neutrons which are incident on the sample will be readily absorbed by the fissile material, and this absorption will depress the interrogation neutron flux in the sample, especially near the sample's center. Additionally, fission neutrons produced near the center of a large sample will have a lesser probability of escaping the sample, which is required in order to detect fission events with the assay chambers. Therefore, the fissile material at the center of the large samples contributes less than the material towards the perimeter of the sample. Hence, the effective fissile mass of a large sample, e.g. a 91g-cylindrical ^{239}Pu sample, will be less than the actual isotopic mass. It's possible to notice a deviation from linearity between the assay of the 47g and 91g samples, which demonstrates that the self-shielding effect is more significant in large fissile samples. However, since the data point corresponding to 138g of ^{239}Pu is simply the assay of both of the previous samples, the result is the sum of the previous points and a return to linearity. Instead, if the last point corresponded to a 138g-cylindrical ^{239}Pu sample, there would be a clear deviation from linearity.

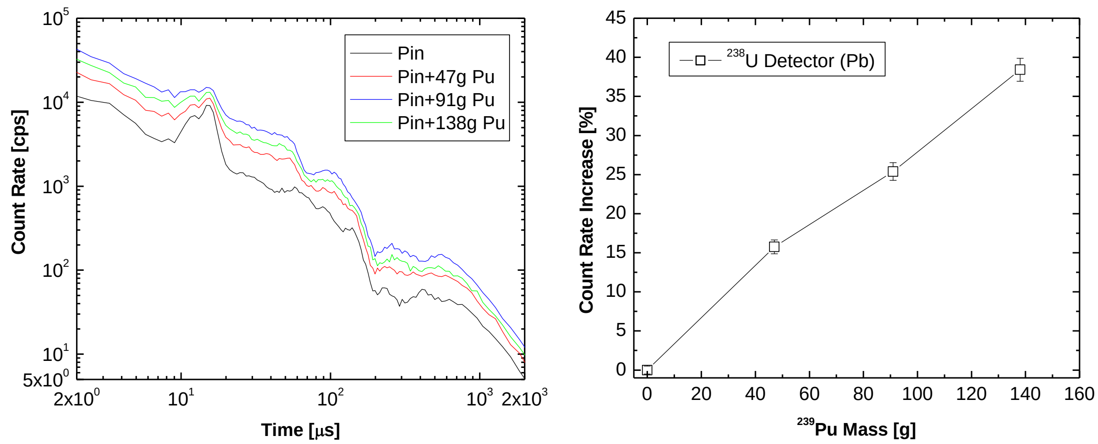

Figure 4.7 Left: ^{238}U Detector (Pb) response as a function of slowing-down time for a fresh SPERT fuel pin with four incremental Pu configurations. Right: Corresponding percent increase of the integrated detector responses (40 to 200μs)

The results in Figure 4.7 (left) clearly show that the interrogation of large increments of fissile Pu results in elevated assay chamber responses. Additionally, Figure 4.7 (right) demonstrates that this effect is proportional to the additional Pu mass. These results demonstrate the potential of an LSDS system to assay an unknown fuel sample for large increments of fissile Pu content. However, an assay system should also be sensitive to small increments of fissile material in order to be effective for SNF assay.

In order to further benchmark the LSDS for spent fuel assay, the responses of the assay chambers due to small increments of fissile U in the presence of large quantities of fissile material was investigated. These measurements were performed with combinations of the small HEU disks in the presence of the SPERT fuel pin and the PuBe sources.

The first measurement used the SPERT fuel pin (34.8 g ^{235}U) as a baseline fissile sample. The responses of the assay chambers were recorded, and the configuration was incrementally varied by adding 0, 5, and 10 HEU disks, which corresponds to an additional ^{235}U mass of 0, 1.3, and 2.6 grams, respectively. The responses of both ^{238}U assay chambers—one in the assembly and the other in the Pb—corresponding to these measurements can be seen in Figure 4.8 and Figure 4.9, respectively.

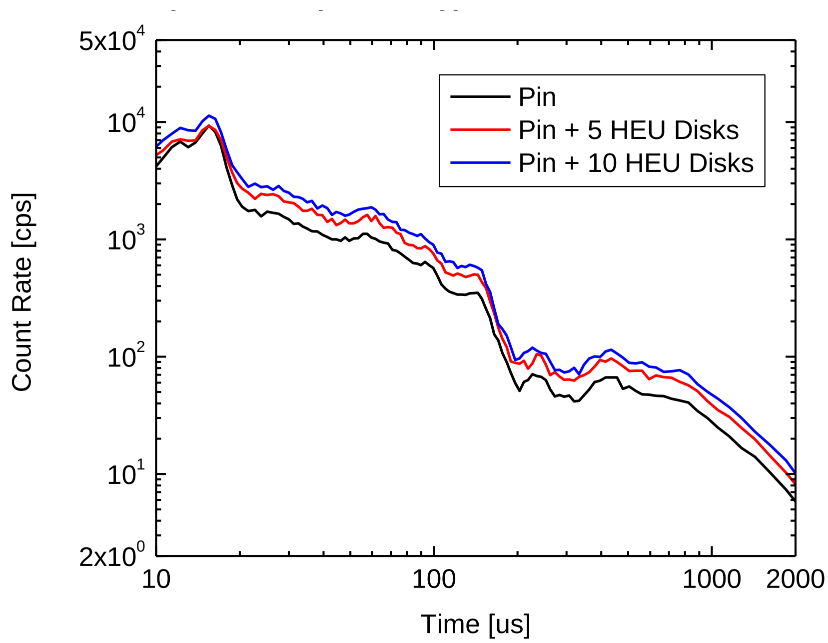

Figure 4.8: ^{238}U Detector (Assembly) response as a function of slowing-down time corresponding to a fresh SPERT fuel pin with variable ^{235}U mass

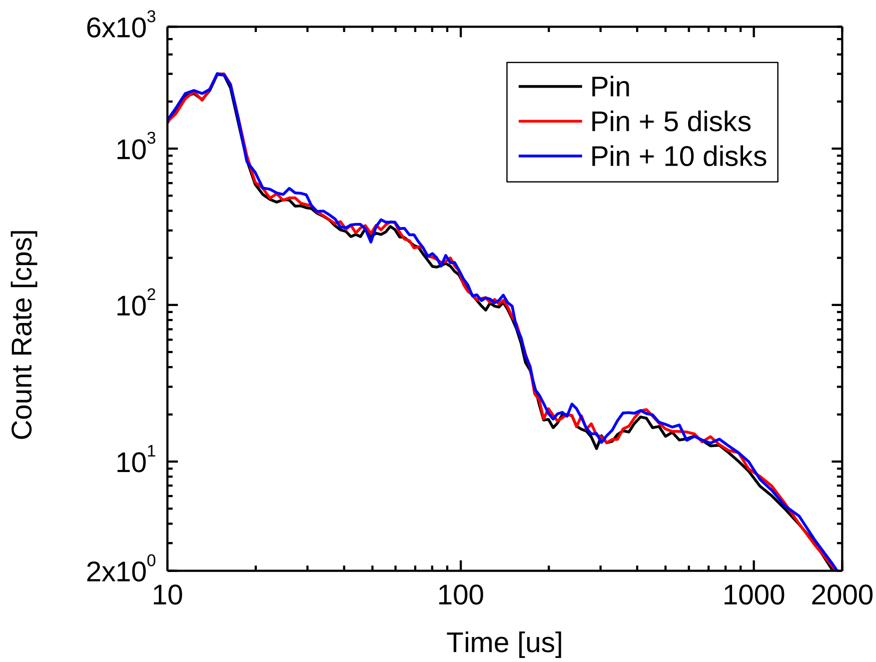

Figure 4.9: ^{238}U Detector (Pb) response as a function of slowing-down time corresponding to a fresh SPERT fuel pin with small, incremental ^{235}U masses

The ^{238}U assay chamber located in the assembly is more sensitive to the additional HEU disks, which is explained by the detector's proximity to the samples. The ^{238}U assay chamber (Pb), on the other hand, is farther from the HEU disks. Therefore, it's more difficult to resolve the individual responses corresponding to this detector for measurements with the small incremental masses. For consistency, the responses of the ^{238}U assay chamber (Pb)—seen in Figure 4.9—were integrated over the region from 40 to 200μs. The integrated results of this measurement corresponding to the ^{238}U assay chamber in the assembly can be seen by the black line of Figure 4.12. This demonstrates that the LSDS is sensitive to small increments of fissile U, even in the presence of large quantities of fissile material.

Subsequently, the sensitivity of the LSDS assay system to the same, small increments of ^{235}U in the presence of large quantities of both ^{235}U and ^{239}Pu was investigated. This time a baseline assay measurement was performed with the SPERT fuel pin and the small PuBe source (47g ^{239}Pu). Afterwards, successive measurements with 0, 5, and 10 HEU disks were attached to the center of the pin. The assay chamber responses were integrated over the same region (40 to 200μs), and the resulting trend can be seen by the red line in Figure 4.12. Next, these measurements were performed with the large PuBe source (91g ^{239}Pu). Later, the measurements were performed yet again with both PuBe sources (138g ^{239}Pu). The responses of the ^{238}U assay chamber (Pb) corresponding to the incremental HEU disks in the presence of both Pu samples can be seen in Figure 4.10. The same responses can be seen in Figure 4.11, which focuses on the ^{235}U resonance region, corresponding to a slowing down time of 20 to 100μs. Again, these responses are difficult to resolve with the ^{238}U assay chamber due to the large baseline fissile mass.

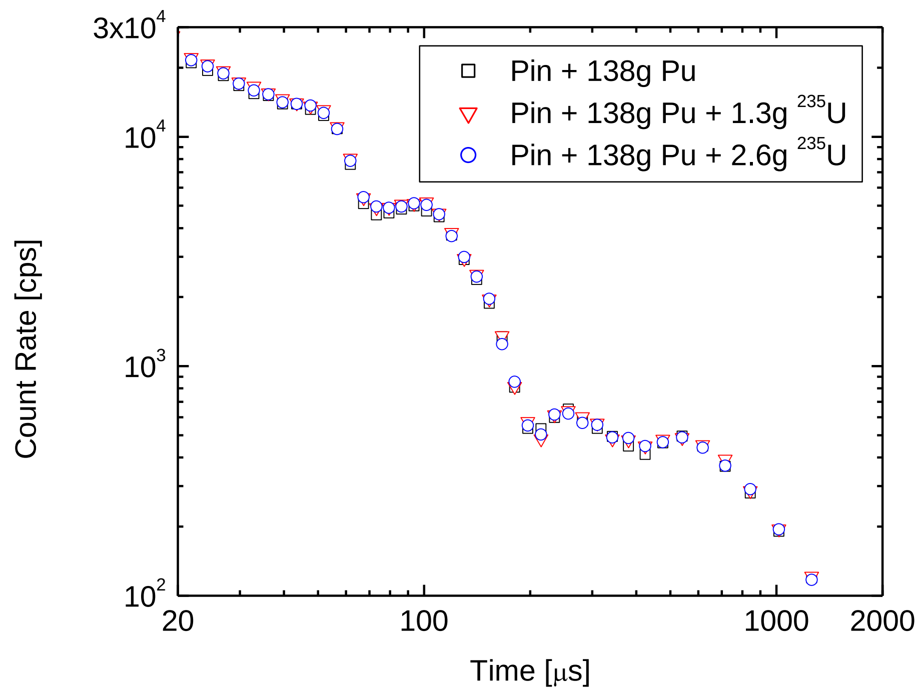

Figure 4.10: ^{238}U assay chamber (Pb) response to incremental ^{235}U disks in the presence of the SPERT fuel pin and both PuBe sources

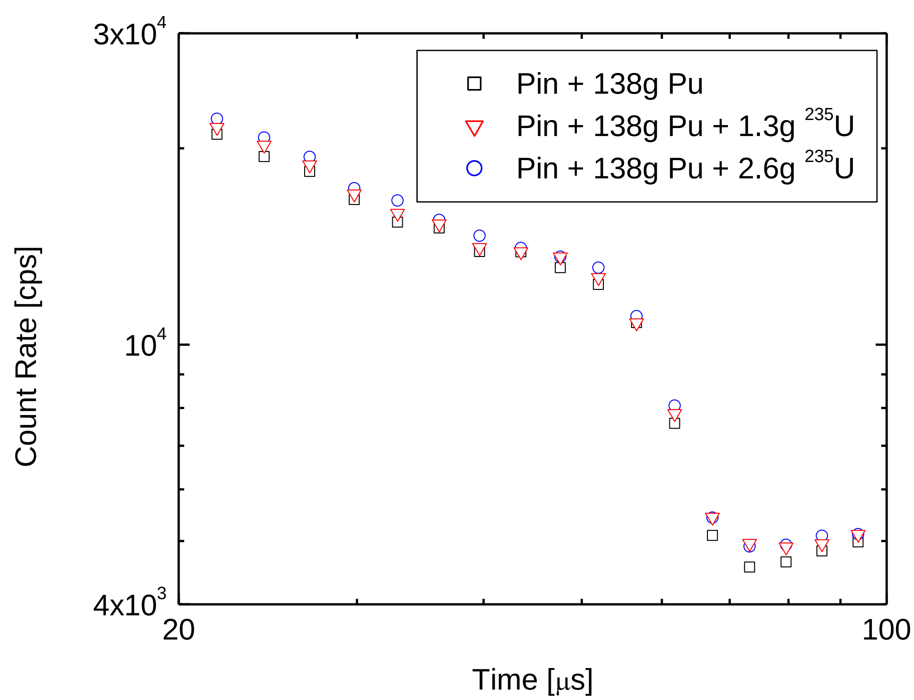

Figure 4.11: ^{238}U assay chamber (Pb) response to incremental ^{235}U disks in the presence of the SPERT fuel pin and both PuBe sources from 20 to 100μs

The integrated responses of the ^{238}U assay chamber (Pb) corresponding to the aforementioned measurements are shown by the left-hand-side of Figure 4.12. This plot depicts the total increase of counts in the aforementioned ^{235}U resonance region due to the small increments of ^{235}U mass. The large relative error is due to the relatively small increase of the integrated count rates in the presence of large background quantities of ^{235}U and ^{239}Pu. The total number of counts added is comparable for the four experimental configurations. The right-hand-side of Figure 4.12 depicts the relative increase of the integrated count rates in the same time window. The relative increase is more significant corresponding to the experiment with just the Pin and incremental ^{235}U disks (no Pu samples), since there is significantly less background fissile material. Both plots in Figure 4.12 demonstrate that the LSDS system is sensitive to small increments of HEU in the presence of large quantities of fissile material. In fact, the aforementioned measurements demonstrate that the LSDS is sensitivity to changes fissile masses corresponding to increments which are less than 1% of the total fissile mass.

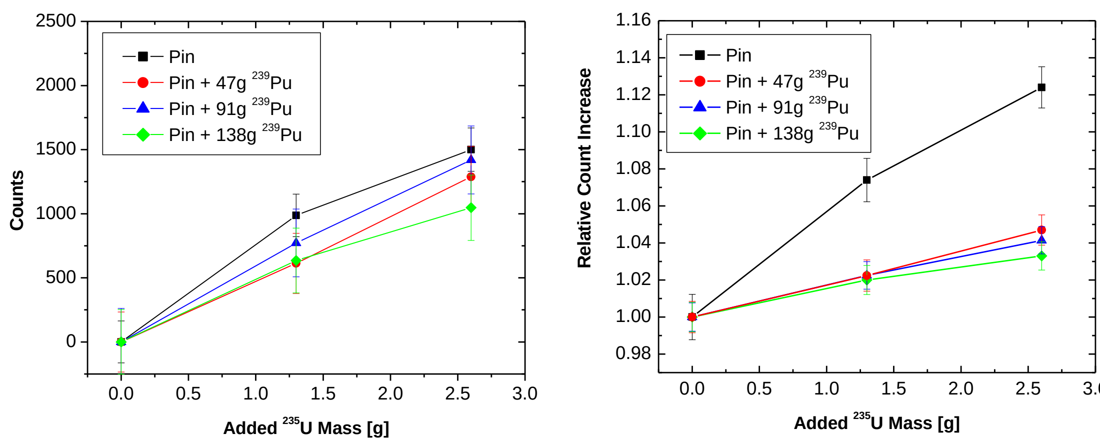

Figure 4.12 (Left): Difference in the integrated response of the ^{238}U assay detector (Pb) due to small incremental ^{235}U masses in the presence of the SPERT fuel pin and various configurations of Pu. (Right): Same responses plotted as relative increases

4.5 Application of Analysis Algorithms

The research focus for the scope of this thesis involved the design, performance, and data acquisition of experiments and the verification of the results with corresponding Monte Carlo simulations. However, a significant part of the collaborative effort of this project involved the analysis of the experimental data in order to quantify the fissile masses within the assayed samples, which was performed by researchers at PNNL. Therefore, a summary of this analysis is included for completion.

Since the geometric configurations of the assayed fissile samples within the RPI LSDS are complex and exhibit self-shielding effects, it was determined that the development of assay algorithms would be the best way to estimate fissile masses with sufficient accuracy. A simplified linear combination is exemplified in equation (8), where R_{SNF} is the assay detector response to an unknown sample of spent nuclear fuel containing both ^{235}U and ^{239}Pu, A and B are the unknown masses of ^{235}U and ^{239}Pu in the SNF, respectively, and $R_{^{235}U}$ and $R_{^{239}Pu}$ are the assay chamber responses to ^{235}U and ^{239}Pu, respectively.

$$R_{SNF} = A * R_{^{235}U} + B * R_{^{239}Pu} \tag{8}$$

An advantage of applying a linear combination algorithm is its empirical nature, i.e. it does not rely on a physical model, including the use of isotopic probe chambers responses. However, while this linear combination works well for small fissile samples—e.g. a single SPERT fuel pin—it falls short when large samples—e.g. an SNF assembly—are assayed due to self-shielding effects.

More complex algorithms were developed at PNNL in order to account for the self-shielding associated with the large fissile samples assayed in the RPI LSDS. A linear empirical algorithm, a quadratic empirical algorithm, and a semi-empirical algorithm were each developed each using the maximum likelihood estimation (MLE). These algorithms were previously applied and successfully tested against MCNP-simulated results of the LSDS assay method [42]. Subsequently, these PNNL algorithms were applied to the aforementioned experimental measurements collected at the RPI Gaerttner LINAC Center [46]. Overall, the linear empirical algorithm performed the best at calculating the ^{235}U and ^{239}Pu mass for seven experimental configurations assayed with the RPI LSDS. A brief description of the linear empirical algorithm developed at PNNL and the results of its application are outlined in the subsequent section for completion.

4.5.1 The Linear Empirical Algorithm

The linear empirical algorithm uses linear algebra to relate a matrix which contains the responses of the assay chambers corresponding to multiple fissile configurations to a matrix containing the isotopic masses of the matching fissile configurations. This relationship is demonstrated by equation (9).

$$\boldsymbol{Y} = \boldsymbol{BM} + \boldsymbol{E} \tag{9}$$

First, a set of calibration measurements are input into equation (9) in order to determine matrix **B**. The matrix **Y** is formed by the assay chamber responses corresponding to k calibration configuration. Thus, **Y** has dimensions of n × k, where n is the number of slowing-down time bins making up each assay detector response and k is the number of calibration configurations. Matrix **M** is a p × k matrix consisting of the known p isotopic masses of interest in k calibration configurations. **B** is an n × p matrix, which is determined by this calibration process. **E** is an n × k matrix containing n offsets, which are determined from the error residuals corresponding to the k calibration configurations. Once matrices **B** and **E** are determined, equation (9) can be used to determine the fissile masses corresponding to the assay of unknown samples. Now, **Y** is a matrix composed of k assay detector responses corresponding to k unknown samples, **B** is the same n × p matrix determined in the previous analysis, **E** is the same n × k matrix, and **M** is the unknown matrix containing the p fissile masses. Solving for matrix **M** provides the individual fissile masses for the unknown sample configurations. The results of the application of this linear empirical algorithm to the experimental measurements can be seen in Table 4.5 and Table 4.6.

Table 4.5: Evaluation of the linear empirical algorithm used to quantify the fissile content of ^{235}U corresponding to experimental measurements with the RPI LSDS

Experimental Configuration	Actual ^{235}U Mass [g]	Fitted ^{235}U Mass [g]	Relative Error [%]
Pin + 5 HEU disks	36.1	36.7	1.6
Pin + 5 HEU disks + small PuBe	36.1	34.9	-3.1
Pin + 10 HEU disks + small PuBe	37.4	37.5	0.3
Pin + large PuBe	34.8	34.9	0.4
Pin + 10 HEU disks + large PuBe	37.4	37.2	-0.6
Pin + both PuBe	34.8	35.4	1.8
Pin + 5 HEU disks + both PuBe	36.1	35.2	-6.0
RMSE	-	-	2.7

Table 4.6: Evaluation of the linear empirical algorithm used to quantify the fissile content of ^{239}Pu corresponding to experimental measurements with the RPI LSDS

Experimental Configuration	Actual ^{239}Pu Mass [g]	Fitted ^{239}Pu Mass [g]	Relative Error [%]
Pin + 5 HEU disks	0	-	-
Pin + 5 HEU disks + small PuBe	47	43.3	-7.9
Pin + 10 HEU disks + small PuBe	47	42.3	-10.1
Pin + large PuBe	91	98.5	8.2
Pin + 10 HEU disks + large PuBe	91	92.5	1.6
Pin + both PuBe	138	140.6	1.9
Pin + 5 HEU disks + both PuBe	138	139.7	1.2
RMSE	-	-	6.3

5. CONCLUSIONS AND FUTURE WORK

This work was funded by the DOE MPACT Campaign in order to order to demonstrate the feasibility of Lead Slowing-Down Spectroscopy (LSDS) for the assay of individual fissile isotopes—i.e. ^{235}U, ^{239}Pu, and ^{241}Pu—in spent nuclear fuel (SNF) assemblies. Due to the radiation safety hazard and high cost associated with the handling of SNF assemblies, it was not possible to demonstrate a proof of principle for the assay of entire assemblies using the LSDS assay method. Instead, experiments were performed at the Gaerttner LINAC Center at RPI with discrete samples of fissile U and Pu in order to mimic the composition of SNF. These measurements demonstrated that the RPI LSDS is sensitive to small increments of fissile U and Pu in the presence of large quantities of fissile material. The experimental data were implemented into a linear empirical analysis algorithm developed at PNNL, which was able to assay the individual fissile isotope masses with a root-mean-square error of 2.7% for ^{235}U and 6.3% for ^{239}Pu [46]. Additional work is necessary to demonstrate a proof of principle for the isotopic assay of SNF assemblies using LSDS, but the experimental results present here demonstrate progress towards that goal.

REFERENCES

[1] T. Moss and D. Sills, "Three Mile Island in Perspective Keynote Address," in *The Three Mile Island Nuclear Accident: Lessons and Implications,* vol. 365, New York, NY, USA: New York Acad. of Sci., 1981, pp. 1-9.

[2] United States Nuclear Regulatory Commission, "Spent Fuel Storage in Pools and Dry Casks," 2012. [Online]. Available: http://www.nrc.gov/waste/spent-fuel-storage/faqs.html, Accessed on Feb. 1, 2013.

[3] National Research Council, "Introduction," in *Nuclear Wastes: Technologies for Separations and Transmutation, Committee on Separations Technology and Transmutation Systems*. Washington, D.C., USA: Nat. Acad. Press, 1996, ch. 1, pp 11-20. [Online]. Available: https://www.nap.edu/read/4912 /chapter/1, Accessed on Apr. 10, 2014.

[4] K. J. Notz. Characteristic of Spent Nuclear Fuel. presented at 4th Int. Symp. on Ceramics in Nucl. Waste Manage. [Online]. Available: http://www.iaea.org/inis /collection/NCLCollectionStore/_Public/20/061/20061554.pdf, Accessed on Mar. 14, 2014.

[5] United States Nuclear Regulatory Commission, "Special Nuclear Material," 2012. [Online]. Available: http://www.nrc.gov/materials/sp-nucmaterials.html, Accessed on Feb. 1, 2014.

[6] United States Nuclear Regulatory Commission, "Nuclear Security and Safeguards," 2012. [Online]. Available: http://www.nrc.gov/security.html, Accessed on Mar. 1, 2012.

[7] Online Etymology Dictionary Website, "Assay," 2001. [Online]. Available: http://etymonline.com/index.php?term=assay&allowed_in_frame=0, Accessed on Apr. 10, 2013.

[8] J. Kulisek, et al. "Update on Establishing the Feasibility of Lead Slowing Down Spectroscopy for Direct Measurement of Plutonium in Used Fuel," Pacific Northwest Nat. Lab., Richland, WA, USA, Rep. PNNL-SA-80557, 2013.

[9] N. Abdurrahman, et al. "Spent-Fuel Assay Performance and Monte Carlo Analysis of the Rensselaer Slowing-Down-Time Spectrometer," *Nucl. Sci. Eng.,* vol. 115, pp. 279-296, Dec., 1993.

[10] D. Cramer, R. Slovacek, E. Bean and R. and Luce, "Lead Spectrometer for Non-Destructive Nuclear Fuel Assay," Knolls Atomic Power Lab., Schenectady, NY, USA, 1976, Rep. KAPL-M-7449, 1976.

[11] S. Tobin, et al. "Determining Plutonium Mass in Spent Fuel with Nondestructive Assay Techniques-Preliminary Modeling Results Emphasizing Integration among Techniques," presented at the 2009 Proc. of Global, Paris, France, Sept. 6-11, 2009.

[12] United States Nuclear Regulatory Commission, Transportation of Spent Nuclear Fuel. [Online]. Available: http://www.nrc.gov/waste/spent-fuel-transp.html, Accessed on May 1, 2013.

[13] United States Nuclear Regulatory Commission, "Materials Transportation Oversight," 2012. [Online]. Available: http://www.nrc.gov/materials/transportation/ oversight.html, Accessed on Apr. 6, 2013.

[14] United States Nuclear Science Committee, "Spent Nuclear Fuel Assay Data for Isotopic Validation," Nucl. Energy Agency: Organisation for Economic Co-operation and Develop., Paris, France, 2011. [Online]. Available: https://www.oecd-nea.org/science/wpncs/ADSNF/SOAR_final.pdf, Accessed on Mar. 22, 2013

[15] M. Scchear, H. Menlove, S. Tobin, L. Evans and S. Lee, "Fissile Material Measurements using the Differential Die-Away Self Interrogation Technique," *Nucl. Instruments and Methods in Physics Res.,* vol. 602, pp. 588-593, Apr. 2009.

[16] L. Campbell, et al., "High Energy Delayed Gamma Spectroscopy for Plutonium Assay of Spent Fuel," Pacific Northwest Nat. Lab., Richland, WA, USA, PNNL-CN-184/128, 2010. [Online]. Available: https://www.iaea.org/safeguards/symposium /2010/Documents/PapersRepository/128.pdf, Accessed on Aug. 1, 2012

[17] J. Kulisek, et al., "Lead Slowing-Down Spectrometery Time Spectral Analysis for Spent Fuel Assay: FY11 Status Report," Pacific Northwest Nat. Lab., Richland, WA, USA, PNNL-20769, 2010. [Online]. Available: https://www.iaea.org/safeguards

/symposium/2010/Documents/PapersRepository/128.pdf, Accessed on Mar. 19, 2012

[18] Y. Lee et al., “Design of a Spent Fuel Assay Devise Using Lead Spectrometer and Neutron Emission Tomography,” Ph.D. dissertation, MANE Dept., RPI, Troy, NY, 1993.

[19] P. Rinard, "Application Guide to Shufflers," Los Alamos Nat. Lab., Los Alamos, NM, USA, LA-13819-MS, Sept. 2001. [Online]. Available: http://www.lanl.gov/orgs/n/n1/docs /la_13819.pdf, Accessed on Jan. 1, 2013

[20] K. A. Jordan and T. Gozani, "Pulsed Neutron Differential Die Away Analysis for Detection of Nuclear Materials," *The Appl. of Accelerator in Res. and Ind.,* vol. 261, no. 1-2, pp. 365-368, Aug. 2007.

[21] J. Atencio, J. Caldwell and W. Kunz, "Apparatus and Method for Quantitative Assay of Generic Transuranic Wastes from Nuclear Reactors," U.S. Patent US4483816, Nov. 20, 1984.

[22] H. Menlove et al., "Fissile and Fertile Nuclear Material Measurements using a New Differential Die-Away Self-Interrogation Technique," *Nucl. Instruments and Methods in Physics Res.,* vol. 602, no. 2, pp. 588-593, Apr. 2009.

[23] N. Ensslin, et al., "Passive Neutron Multiplicity Counting,” Los Alamos Nat. Lab., Los Alamos, NM, USA, LA-UR-07-1402, 1998.

[24] N. Ensslin, W. Harker, M. Krick, D. Langner, M. Pickrell and J. Stewart, "Application Guide to Neutron Multiplicity,” Los Alamos Nat. Lab., Los Alamos, NM, USA, LA-13422, 1998.

[25] D. Lee and L. Lindquist, "Self-Interrogation of Spent Fuel," Los Alamos Nat. Lab., Los Alamos, NM, USA, LA-9494-MS, 1982. [Online]. Available: http://www.iaea.org/inis/collection/NCLCollectionStore/_Public/14/734 /14734049.pdf?r=1, Accessed on Sept. 1, 2013

[26] S. De La Cruz, "Computational Study of Passive Neutron Albedo Reactivity (PNAR) Measurement with Fission Chambers," M.S. thesis, Univ. of NV Las Vegas, Las Vegas, NV, 2011.

[27] A. LaFleur, "Development of Self-Interrogation Neutron Resonance Densitometry (SINRD) to Measure the Fissile Content in Nuclear Fuel," Ph.D dissertation, Dept. of Nucl. Engr., Texas A&M University, Coll. Station, TX, USA, 2011.

[28] A. LaFleur, W. Charlton, H. Menlove and M. Swinhoe, "Nondestructive Measurements of Fissile Material using Self-Indication Neutron Resonance Absorption Densitometry (SINRAD)," presented at the *8th Int. Conf. on Faculty Op.-Safeguards Interface*, Portland, OR, Mar. 30-Apr. 4, 2008.

[29] A. LaFleur, W. Charlton, H. Menlove and M. Swinhoe, "Comparison of Fresh Fuel Experimental Measurements to MCNPX Calculations Using Self-Interrogation Neutron Resonance Densitometry," *Nucl. Instru. and Methods in Physics Res. A,* vol. 680, no. 11, pp. 168-178, July 2012.

[30] S. Tobin, J. Conlin, L. Evans and J. Hu, "Determining Plutonium Mass in Spent Fuel with Non-Destructive Assay Techniques," Los Alamos Nat. Lab., Los Alamos, NM, USA, LA-UR-10-06243, 2010.

[31] L. Campbell, E. Smith and A. Misner, "High-Energy Delayed Gamma Spectroscopy for Spent Nuclear Fuel Assay," *IEEE Trans. on Nucl. Sci.,* vol. 58, no. 1, pp. 231-240, Feb. 2011.

[32] V. Mozin, S. Tobin, A. Hunt and J. Vujic, "Delayed Gamma Technique for Fissile Material Assay," Los Alamos Nat. Lab, Los Alamos, NM, USA, LA-UR-10-04701, Jan. 2010.

[33] U. Kneissl, H. Pitz and A. Zilges, "Investigation of Nuclear Structure by Resonance Fluorescence Scattering," *Prog. Part. Nucl. Physics,* vol. 37, pp. 349-422, Dec. 1996.

[34] B. Quiter, A. Ludewigt, and S. D. Ambers, "Assessment of Nuclear Resonance Fluorescence for Spent Nuclear Fuel Assay," Univ. of Cal., Berkley and Lawrence Berkely Nat. Lab., Berkely, CA, USA 2012. [Online]. Available: https://www.osti.gov /scitech/servlets/purl/1045925, Accessed on Dec. 14, 2013

[35] E. Gaerttner, M. Yeater and R. Fullwood, "Rensselaer Polytechnic Institute LINAC Facility," presented at the Proc. of Symp. on Neutron Phys., Troy, NY, USA, May 5-6, 1961.

[36] C. Romano, Y. Danon, R. Block, E. Blain and E. and Bond, "Measurements of Fission Fragment Properties using RPI's Lead Slowing Down Spectrometer," presented in Int. Conf. on Nucl. Data for Sci. and Tech., Nice, France, Apr. 22-27, 2007.

[37] C. Romano, et al., "Fission Fragment Mass and Energy Distributions as a Function of Incident Neutron Energy Measured in a Lead Slowing-Down Spectrometer," *Physical Rev C*, vol 81, no. 1, pp 1-11, Jan. 2010.

[38] R. Slovacek, D. Cramer and E. Bean, "U-238 (n,f) Measurements Below 30 keV," presented at the Meeting of the Amer. Physical Soc., Washington, D.C., USA, Apr. 28, 1974.

[39] R. Block, "Neutron Spectroscopy with the Rensselaer Intense Neutron Spectrometer," RPI, Troy, NY, USA, Rep. COO-2494-10, 1978.

[40] M. Williams, *The Slowing Down and Thermalization of Neutrons.* Amsterdam, Holland: North-Holland Pub. Co., 1966, pp 111-144.

[41] J. Thompson and Y. Danon, "Development of a New Method to Measure (n,alpha) and (n,p) Cross Sections Using a Lead Slowing-Down Spectrometer," presented at the Amer. Nucl. Soc. Conf., Knoxville, TN, USA, Apr. 3-7, 2011.

[42] J. Kulisek et al., "Lead Slowing-Down Spectrometry Time Spectral Analysis for Spent Fuel Assay: FY12 Status Report," Pacific Northwest Nat. Lab., Richland, WA, USA, PNNL-219702012. [Online]. Available: http://www.pnnl.gov/main/publications /external /technical_reports/PNNL-21970.pdf, Accessed on Feb. 27, 2012

[43] Los Alamos National Laboratory MCNPx Website. [Online]. Available: https://mcnpx.lanl.gov/, Accessed on January 21, 2016.

[44] National Nuclear Security Administration Sageguards Initiative Website. [Online]. Available: http://nnsa.energy.gov/mediaroom/factsheets/nextgenerationsafeguards, Accessed on Apr. 23, 2016.

[45] B. Becker, A. Weltz, J. Kulisek, J. Thompson and N. Thompson, "Non-destructive Assay Measurements Using the RPI Lead Slowing Down Spectrometer," *Nucl. Sci. and Engr.* vol. 175, no. 2, pp. 124-134, Feb. 2013.

[46] G. A. Warren, et al., "Lead Slowing-Down Spectrometry Analysis of Data from Measurements on Nuclear Fuel," *Nucl. Sci. and Eng.,* vol. 179, no 3., pp. 1-10, Mar. 2015.

APPENDIX 1: Special Nuclear Material License—RPI
https://www.nrc.gov/docs/ML1219/ML121920732.pdf

APPLICATION FOR NEW LICENSE
SPECIAL NUCLEAR MATERIALS

Submitted to
Director, Fuel Facility Licensing Directorate Division of Fuel Cycle Safety and Safeguards
Office of Nuclear Material Safety and Safeguards
U.S. Nuclear Regulatory Commission
Washington, D.C. 20555

by

Office of Radiation and Nuclear Safety
Rensselaer Polytechnic Institute
110 8th Street
Troy, NY 12180-3590

Revision 3
March 27, 2012

1) 10 CFR 70.22(a)(1) Name of Applicant

Office of Radiation and Nuclear Safety
Rensselaer Polytechnic Institute
110 8th Street
Troy, NY 12180-3590

Peter F. Caracappa, Ph.D., CHP
Radiation Safety Officer
NES 1-19
US Citizen
Yaron Danon, Ph.D.
Director, Linear Accelerator Laboratory
NES 1-9
Citizen of Israel

Curtis Powell, SHRM
Vice-President, Division of Human Resources
Gurley Building
21 Union Street
Troy, NY 12180
US Citizen

David V. Rosowsky, Ph.D.. P.E., F. ASCE
Dean, School of Engineering
JEC 3018
US Citizen

2) 10 CFR 70.22(a)(2) Activity and location for which Special Nuclear Material License is requested

Rensselaer Polytechnic Institute is requesting permission to possess a total of 64 SPERT F-1 fuel pins containing uranium enriched to 4.81 weight percent U-235, each containing 35.2 grams U- 235, at its Linear Accelerator facility on its campus for the purpose of demonstrating methods to assay spent nuclear fuel for fissile material inventory.

RPI possesses and uses Special Nuclear Material for a variety of teaching and research purposes under License #1035 from the New York State Department of Health. The Special Nuclear Material inventory consists mainly of Plutonium-Beryllium sources that are used to produce neutrons and uranium enriched in U-235 used for nuclear cross-section measurements. RPI is requesting that all special nuclear material possessed at the RPI LINAC be transferred to this newly requested SNM license.

RPI also possesses and uses Special Nuclear Material in the form of SPERT F-1 fuel pins at the 3 Walthousen Laboratory, which is a licensed critical assembly operating under NRC license CX- 22. The material covered under this license request will be obtained through transfer of excess unused fuel pins from the CX-22 license to this newly requested SNM license.

The LINAC Laboratory facility is physically located at
3021 Tibbets Ave,
Troy, NY 12180.

A diagram of the facility location and floor plan is included in Appendix A. The primary location for storage of the special nuclear materials when not in use will be in the location labeled "Hot Cell", and the material will be used in the Lead Slowing Down Spectrometer, in the area labeled "Target Room." Two PuBe sources associated with this license may be used in other experimental areas within the boundaries of the facility as required.

3) 10 CFR 70.22 (a)(3) Requested duration of license is for 10 years.

4) 10 CFR 70.22(a)(4) Description of Special Nuclear Material

A. Description of Material

1) The material requested under this license consists of 64 SPERT (F-1) fuel pins qualified by the DOE (EGG-NTA-766, R. R. Hobbins) for use in a non-power reactor assembly. Each fuel pin is made up of sintered UO2 pellets, encased in a stainless steel tube, capped on both ends with a stainless steel cap and held in place with a chromium-nickel spring. An aluminum oxide (Al2O3) insulator between the fuel pellets and stainless steel caps on each end of the rod is installed. Gas gaps to accommodate fuel expansion are also provided at both the upper end and around the fuel pellets. Figure 1 depicts a single fuel pin and its pertinent dimensions. Tables 1 through 3 provide detailed compositions of the fuel pins.

2) Two PuBe sources currently possessed under NYSDOH License #1035 will be transferred to this license: • Source #MRC-330 (50g element/47g isotope) • Source #963-S-55 (96g element/91g isotopes) Both items consist of a plutonium-beryllium matrix in doubly encapsulated steel

3) A set of 195 uranium metal disks and a 12 in2 metal foil, enriched in U-235 (64g element/60g isotope). 4 Table 1: Measurements and Specifications for SPERT (F-1) Fuel 5 Table 2: Composition of Uranium Oxide Fuel Table 3: Composition of Stainless Steel Clad 6

Table 1: Measurements and Specifications for SPERT (F-1) Fuel

	Argonne Requalification Data	Phillips Idaho Specifications
Clad OD (in.)	0.4656±0.0007	0.463-0.468
Clad ID (in.)		0.4255-0.4265
Clad Length (in.)	41 5/8	
Weld regions OD (in.)	0.4726±0.0015	0.463-0.468
Fill gas	He + H_2, 0.6 - 3.3 psig	He, 1 psig
UO_y density (g/cm^3), ρ	10.078±0.0037	>9.97 g/cm^3 mean ±0.10 g/cm^3
UO_y diameter (in.)	0.4200±0.001	0.4025-0.4195
UO_y stack length (in.)	35.982±0.01	35.938-36.062
UO_y composition		
w/o U233	0.0003±0.0005	
w/o U234	0.0253±0.0005	
w/o U235	4.8074±0.001	2-5
w/o U236	0.0468±0.0005	
w/o U238	95.1202±0.002	
w/o U in oxide, W	87.916±0.018	
[illegible]	2.041±0.003	2.00-2.02
Ca (ppmw)	38±(3-10%)	<100
Cr (ppmw)	13±(3-10%)	<500
Fe (ppmw)	66±(3-10%)	<1200
Mg (ppmw)	10±(3-10%)	<20
Ni (ppmw)	10±(3-10%)	<300
Impurity $\Sigma_{athermal}$ (cm-1)	0.00006 (calculated)	<0.0010
SS304 Composition		
w/o Co	0.084±(3-10%)	<0.05
w/o Cr	18.60±(1-5%)	ASTM A-269-62T
w/o Cu	0.17±(1-5%)	<0.50
w/o Fe	68.9±(1-5%)	ASTM A-269-62T
w/o Mu	1.06±(1-5%)	ASTM A-269-62T
w/o Mo	0.20±(1-5%)	0.50
w/o Ni	9.56±(1-5%)	ASTM A-269-62T
w/o B	-----	<0.005

Table 2: Composition of Uranium Oxide Fuel

	ϵ_j (w/f)	x_j (a/f)	Concentrations C_j (1/bcm)
U233	0.000003	0.000003	0.00000007±160%
U234	0.000253	0.000257	0.00000577±2%
U235	0.048074	0.048659	0.00109131±0.047%
U236	0.000468	0.000472	0.00001058±1.1%
U238	0.951202	0.950609	0.02132011±0.043%
O			0.04577310±0.15%
Fe			0.00000742±(3-10%)

Table 3: Composition of Stainless Steel Clad

	ϵ_j (w/f)	x_j (a/f)	Concentrations C_j (1/bcm)	Atom fraction
Fe	.70326*	.0125926	.0591497	Fe 0.693188
Cr	.1860	.0035772	.0168027	Cr 0.200983
Ni	.0956	.0016289	.0076512	Ni 0.091513
Mn	.0106	.0001929	.0009063	Mn 0.010840
Mo	.0020	.0000209	.0000977	Cu 0.001503
Cu	.0017	.0000268	.0001257	Mo 0.001171
Co	.00084	.0000143	.0000669	Co 0.000802

*The measured value is 0.689; the value 0.70326 makes $\sum_j \epsilon_j = 1$.

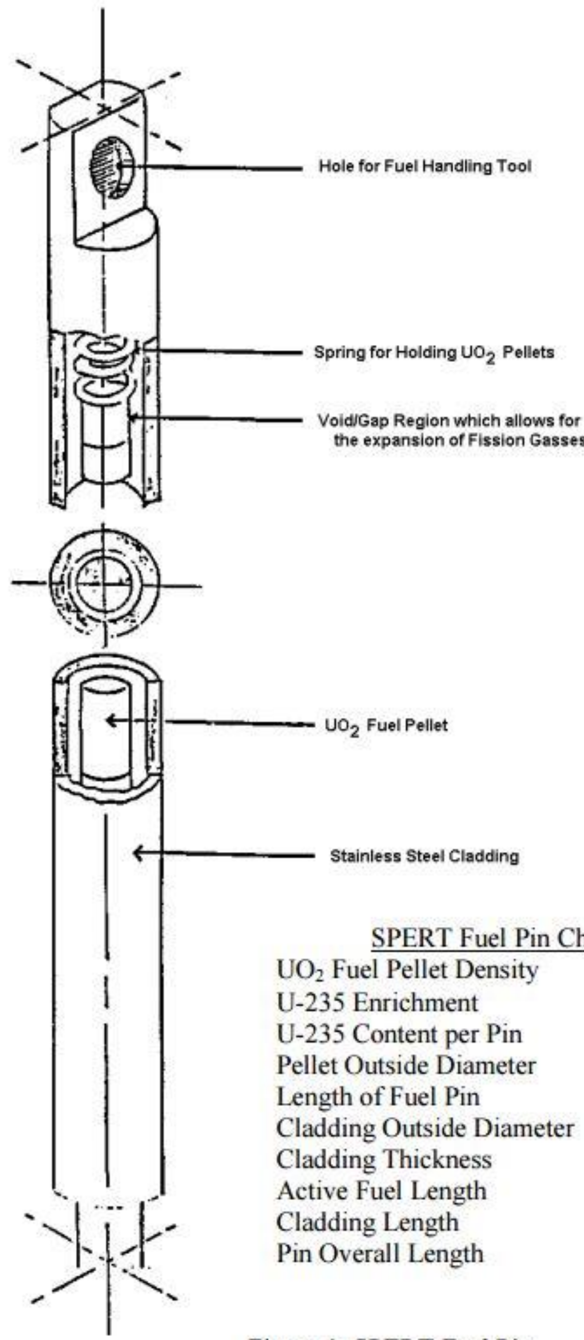

SPERT Fuel Pin Characteristics

UO_2 Fuel Pellet Density	10.08 gm/cm^3
U-235 Enrichment	4.81±0.15 w/o
U-235 Content per Pin	35.2 gm
Pellet Outside Diameter	0.420 in
Length of Fuel Pin	41.75 in
Cladding Outside Diameter	0.466 in
Cladding Thickness	0.020 in
Active Fuel Length	36.00 in
Cladding Length	41.62 in
Pin Overall Length	41.75 in

Figure 1: SPERT Fuel Pin

APPENDIX 2: Sample MCNP Input of the RPI LSDS

```
New Fuel pin
c Radius = Pin radius +0.3 cm
c
c cell cards
99  0 1 IMP:N=0                          $VOID
1   1 -11.34  -1  14 IMP:N=1              $Lead rest
c
100  1 -11.34  -1 13 -14  -15 IMP:N=1         $lead zone 5a
110  1 -11.34  -1 12 -13  -15 IMP:N=3         $lead zone 4a
120  1 -11.34  -1 11 -12  -15 IMP:N=4         $lead zone 3a
130  1 -11.34  -1 10 -11  -15 IMP:N=8         $lead zone 2a
140  1 -11.34  -1 3  -10  -15 #300 #301 IMP:N=10         $lead zone 1a
101  1 -11.34  -1 13 -14  -16 15 IMP:N=1       $lead zone 5b
111  1 -11.34  -1 12 -13  -16 15 IMP:N=2       $lead zone 4b
121  1 -11.34  -1 11 -12  -16 15 IMP:N=4      $lead zone 3b
131  1 -11.34  -1 10 -11  -16 15 IMP:N=5       $lead zone 2b
141  1 -11.34  -1 3  -10  -16 15 #300 #301 IMP:N=10  $#300 #301 lead zone 1b
102  1 -11.34  -1 13 -14   16 IMP:N=1         $lead zone 5c
112  1 -11.34  -1 12 -13   16 IMP:N=2         $lead zone 4c
122  1 -11.34  -1 11 -12   16 IMP:N=4         $lead zone 3c
132  1 -11.34  -1 10 -11   16 IMP:N=8         $lead zone 2c
142  1 -11.34  -1 3  -10   16 #300 #301 IMP:N=10   $lead zone 1c
c
300   0   -304    trcl=(-36.5 -15 52.5) IMP:N=25    $ detector in lead center
301   0   -304    trcl=(-33.5 -15 52.5) IMP:N=25    $ detector in lead right
c
2   0         -3 4  IMP:N=10
3   4  -2.7    (-4 5):-6:-7:-8:-9 IMP:N=10                 $ Al Box
c
c  +++Change for Pu setup++++++
c Both PuBe
c
=================================================
4   4  -2.7    -4 -310 311
            #3 #5 #244 #245 #346 #347 #248 #249 #250 #251
            #344 #345 #246 #247 #348 #349
            #444 #448 #450 #550 #544 #548 IMP:N=10
5   0         -5 17 -18 (310:-311) #3
             #244 #245 #346 #347 #248 #249
             #250 #251 #344 #345 #246 #247 #348 #349
             #444 #448 #450 #544 #548 #550 IMP:N=10
c
=================================================
c
```

```
c
c
6   0          -5 #3 -17 IMP:N=10                           $ below pins
7   0          -5 #3  18 IMP:N=10                           $ above pins
c
244 5  -2.7    -240 241 17 -18   trcl=(-32.5 0 46.5) IMP:N=10  $ Detector Pipe
245 5  -2.7    -240 241 17 -18   trcl=(-40.5 0 46.5) IMP:N=10  $ Detector Pipe
c
c
c  ++++Both PuBe Sources+++++++
c
==================================================
246 40 -1.84   -305         trcl=(-40.5 -4 38.5) IMP:N=100  $PuBe large left
247 40 -2.1    -306         trcl=(-32.5 -3.5 38.5) IMP:N=100 $PuBe small right
c
==================================================
c
c
248 0          -241 17 -18 #346 trcl=(-40.5 0 46.5) IMP:N=10  $
249 0          -241 17 -18 #347 trcl=(-32.5 0 46.5) IMP:N=10  $
c
250 5  -2.7    -302 303 17 -18 trcl=(-36.5 0 42.3685) IMP:N=20    $ Pipe
251 0             -303 17 -18  trcl=(-36.5 0 42.3685) fill=1 IMP:N=20  $ Pipe
c
344 5  -2.7    -240 241 17 -18   trcl=(-32.5 0 38.5) IMP:N=10    $ Detector Pipe
345 5  -2.7    -240 241 17 -18   trcl=(-40.5 0 38.5) IMP:N=10    $ Detector Pipe
346 0         -304     trcl=(-40.5 -12.5 46.5) IMP:N=100  $ Assembly Assay Det
347 0         -304     trcl=(-32.5 -12.5 46.5) IMP:N=100  $ Assembly Assay Det
c
c
c  +++Both PuBe Sources++++++
c
==================================================
348 0          -241 17 -18 #246 trcl=(-40.5 0 38.5) IMP:N=10
349 0          -241 17 -18 #247 trcl=(-32.5 0 38.5) IMP:N=10
c
==================================================
c
c
c FLUX MONITOR U5 (Bottom)
444 0 -600 601 17 -18  trcl=(-36.5 0 39) IMP:N=10
448 0          -601 17 -18 #450 trcl=(-36.5 0 39) IMP:N=10
450 0         -602       trcl=(-36.5 5.5 39) IMP:N=100  $ flux cell bottom left
c
c FLUX MONITOR PU9 (Top)
544 5 -2.7 -600 601 17 -18  trcl=(-36.5 0 46) IMP:N=10
548 0          -601 17 -18 #550 trcl=(-36.5 0 46) IMP:N=10
```

```
550 0     -602              trcl=(-36.5 5.5 46) IMP:N=100  $ flux cell bottom left
c
c
c  +++PIN Setup++++++
c
==============================================================
206   53 -8.0        -202 203 -205      u=1  trcl=(0  51.73 -1.2)  IMP:N=30  $plug
207   54 -3.9        -203 204 -208      u=1  trcl=(0  51.73 -1.2)  IMP:N=30  $spacer
208   53 -8.0        -203 213 -205 208  u=1  trcl=(0  51.73 -1.2)  IMP:N=30  $cladding
209   55 -17.8e-5    -204 206 -208 207  u=1  trcl=(0  51.73 -1.2)  IMP:N=30  $gap (He)
210   52 -10.49      -204 206 -207      u=1  trcl=(0  51.73 -1.2)  IMP:N=60  $Fuel
212   54 -3.9        -206 210 -208      u=1  trcl=(0  51.73 -1.2)  IMP:N=30  $insulator
213   53 -8.0        -210 211 -208      u=1  trcl=(0  51.73 -1.2)  IMP:N=30  $spacer
214   56 -1.0        -211 212 -208      u=1  trcl=(0  51.73 -1.2)  IMP:N=30  $spring
215   53 -8.0        -212 213 -208      u=1  trcl=(0  51.73 -1.2)  IMP:N=30  $plug
216   57 -4.11       -213 214 -205      u=1  trcl=(0  51.73 -1.2)  IMP:N=30 $top of pin
217   0  (205:-214:202)   #220 #221 #222 #223 #224 #225 #226 #227 #228 #229
                 u=1  trcl=(0  51.73 -1.2)  IMP:N=30
c
===============================================================
c
c
c  +++5 Disk setup++++++
c
==============================================================
220   995 -19.05      -500        u=1  trcl=(0 -3.5 -0.5) IMP:N=50
221   995 -19.05      -501        u=1  trcl=(0 -1.5 -0.5) IMP:N=50
222   995 -19.05      -502        u=1  trcl=(0 0.5 -0.5)  IMP:N=50
223   995 -19.05      -503        u=1  trcl=(0 2.5 -0.5)  IMP:N=50
224   995 -19.05      -504        u=1  trcl=(0 4.5 -0.5)  IMP:N=50
225   995 -19.05      -505        u=1  trcl=(0  6.5 -0.5) IMP:N=50
226   995 -19.05      -506        u=1  trcl=(0  8.5 -0.5)  IMP:N=50
227   995 -19.05      -507        u=1  trcl=(0  10.5 -0.5) IMP:N=50
228   995 -19.05      -508        u=1  trcl=(0  12.5 -0.5)  IMP:N=50
229   995 -19.05      -509        u=1  trcl=(0  14.5 -0.5)  IMP:N=50
c
================================================================
c
c
c 500 0 -500 -501 502 trcl=2 IMP:N=100

c cube Surface Cards
1    BOX  -90   -90 -90 180 0 0  0 180 0  0 0 180
2    BOX  -90.1 -90.1 -90.1 180.2 0 0  0 180 0  0 0 180    $Cd Shell
3    BOX  -44    -90 35    15   0 0 0 145 0 0 0 15   $ Assay port
4    BOX  -43.65 -55 35.25 14.5 0 0 0 110 0 0 0 14.5 $ box out
5    BOX  -43.35 -55 35.55 13.9 0 0 0 110 0 0 0 13.9 $ box in
```

```
6    BOX  -43.35 -55 35.55  0.6 0 0 0 110 0 0 0  0.6 $ Al corner
7    BOX  -43.35 -55 49.45  0.6 0 0 0 110 0 0 0 -0.6 $ Al corner
8    BOX  -29.45 -55 35.55 -0.6 0 0 0 110 0 0 0  0.6 $ Al corner
9    BOX  -29.45 -55 49.45 -0.6 0 0 0 110 0 0 0 -0.6 $ Al corner
c
10   C/Y  -36.5  42.5  12
11   C/Y  -36.5  42.5  20
12   C/Y  -36.5  42.5  30
13   C/Y  -36.5  42.5  40
14   C/Y  -36.5  42.5  50
15   PY  -30
16   PY   30
17   PY   -53.0225
18   PY    53.0225
19   PZ   50
c
c fuel pin
c 201  BOX  0 -53.0225 0  1.6256 0 0  0 171.78 0  0 0 1.6256
201  RPP     -0.8128 0.8128 -103.46 0  -0.8128 0.8128
c
C     Pin stuff
202   py       0.0
203   py      -0.9        $top of bottom plug
204   py      -1.22       $Top of bottom spacer
205   cy       0.59182    $clad O.D.
206   py     -92.66       $top of fuel region
207   cy       0.5334     $Fuel pellet radius
208   cy       0.54102    $Gap radius
c    Upper pin stuff
210   py      -92.98
211   py      -93.3
212   py      -98.38
213   py     -100.28
214   py     -103.46
c
500 rcc 0 0 0  0 0 1.0900E-02 0.635
501 rcc 0 0 0  0 0 1.122E-02 0.635
502 rcc 0 0 0  0 0 1.0546E-02 0.635
503 rcc 0 0 0  0 0 1.0474E-02 0.635
504 rcc 0 0 0  0 0 1.0314E-02 0.635
505 rcc 0 0 0  0 0 1.0262E-02 0.635
506 rcc 0 0 0  0 0 1.2622E-02 0.635
507 rcc 0 0 0  0 0 1.0826E-02 0.635
508 rcc 0 0 0  0 0 1.0434E-02 0.635
509 rcc 0 0 0  0 0 1.1418E-02 0.635
c
230  RCC  0  -10. 0  0  20. 0    1.25       $ detector 1 hole
```

```
240  CY    2                    $ detector pipe outside
241  CY    1.8                  $ detector pipe inside
302  CY   1.905                 $ Source Pipe
303  CY   1.8161                $ Source Pipe
c
304  RCC 0 0 0  0 24.2 0    1.27       $ flux cell
305  RCC 0 0 0  0 8.3 0    1.7       $ PuBe Large
306  RCC 0 0 0  0 6.5 0    1.3       $ PuBe Small
c
c FLUX MONITOR PORTs
c
600 CY    .69
601 CY    .55
602 RCC 0 -10 0  0 20 0    .5       $ flux cell
c
310  py   0.15
311  py  -0.15
c
400  BOX 0 -90 0  5.08 0 0 0 30.48 0 0 0 15 $ Lead Brick
c

c -- Transfomations
c tr1  -36.5  51.73 43.35
tr1  0  51.73 0
tr2 -1.2 51.73 0
c
c Material specifications
c lead
M1     82204 -1.37808E-02
       82206 -2.39555E-01
       82207 -2.20743E-01
       82208 -5.25921E-01
       1001 -1E-6   $ 2 ppm H2
       nlib=70c
c
M21   48106   -1.25        $Cd
      48108   -0.89
      48110  -12.49
      48111  -12.80
      48112  -24.13
      48113  -12.22
      48114  -28.73
      48116   -7.49
      nlib=70c
c
c fuel 4.807 w% / 4.868 at% enrichment
C     fuel
```

```
M52   92238 -0.839
      92235 -0.042
      8016  -0.119
      nlib=.70c
C
C     stainless steel
m53    26056  0.69500    24052  0.19000    28058  0.09500    25055  0.02000
      nlib=70c
C
C     Al2O3 Spacers
m54    13027  0.4        8016   0.6
      nlib=70c
C
C     Gas Plenum
m55    1001  0.5         2004  0.5
      nlib=70c
C
C     Spring Region
m56    26056  0.69500   24052  0.19000    28058  0.09500     25055  0.02000
      nlib=70c
C
C     Top of pin (SS comp=SS*0.674)
m57    26056  0.46843 $ 0.69500*0.674
      24052  0.12806 $ 0.19000*0.674
      28058  0.06403 $ 0.09500*0.674
      25055  0.01348 $ 0.02000*0.674
      nlib=70c
c
c
M4     $ BOX
       13027          9.8087E-01
       14028          5.3259E-03
       14029          2.7044E-04
       14030          1.7827E-04
       29063          8.2391E-04
       29065          3.6723E-04
       12024          8.7856E-03
       12025          1.1122E-03
       12026          1.2246E-03
       24050          4.5181E-05
       24052          8.7126E-04
       24053          9.8794E-05
       24054          2.4592E-05
       nlib=70c
c
M5     $ Aluminum 6061
       13027          -97.375
```

```
      14028          -0.55338
      14029          -0.02802
      14030          -0.0186
      26054          -0.0203
      26056          -0.32102
      26057          -0.0077
      26058          -0.00098
      29063          -0.1901625
      29065          -0.0848375
      25055          -0.075
      12024          -0.7899
      12025          -0.1
      12026          -0.1101
      24050          -0.00869
      24052          -0.167578
      24053          -0.019002
      24054          -0.00473
      30000          -0.125
      22046          -0.006
      22047          -0.005475
      22048          -0.05535
      22049          -0.004125
      22050          -0.00405
      nlib=70c
c
M40     $ PuBe13 source
        94239.70c   -84.24
        94240.70c    -5.31
        94242.70c    -0.09
        95241.70c    -0.36   $ Pu241 decayed to Am241
        4009.70c    -48.46
c
M992 90232.70c 1
M995 92235.70c 1
M998 92238.70c 1
M9982 92238.70c 1          $ ENDFb VII
     92235.70c 4.1E-6
c M 92238.31c 1          $ JEFF31 XS
c      92235.70c 4.1E-6
M999 94239.70c 1           $ 3 mg Pu239 detector
c
c
c source specification etc.
c
MODE N
CUT:N   2E5    1E-10          $Energy Cut-off at 0.1 eV, Time Cut-off at approx. 100 us
nps 9e8
```

```
prdmp j 3e8 1 2 9e7
print -128
c
c sources
c
sdef ERG=D1 tme=d2
SP1 -5 0.46                    $Source distribution
si2   -4.9 4.9
sp2    0    1
c
c
c Tallies
C
FC4 Assay det. bottom left F5 U238 Cell 246
F4:N  346 347  t                        $Point detector 4
FM4    (5.0606E-4  9982  -6)
fq4  t e
c
FC14 U235 Flux Monitor
F14:N  450                     $Point detector 4
FM14    (1.63e-7  995  -6)
fq14  t e
c
FC24 Pu239 Flux Monitor
F24:N  550                     $Point detector 4
FM24    (4.8122e-8  999  -6)
fq24  t e
c
FC34 U238 Assay Lead
F34:N  300                     $Point detector 4
FM34    (5.0606E-4  9982  -6)
fq34  t e
E34:N 0.1 0.2 0.3 0.4 0.5 0.6 0.7 0.8 1 2 20  $Energy Cutoff Card
c
FC44 Th Assay Lead
F44:N  301                     $Point detector 4
FM44    (5.1915E-4 992 -6)
fq44  t e
c
```